

# Ubiquitous Molecular Outflows in z□>□4 Massiv@usty Galaxies.I. Sample Overview and Clumpy Structure in Molecular Outflows on 500 pc Scales

Justin S.Spilker<sup>1,18</sup>, Kedar A. Phadke, Manuel Araven, Matthieu Béthermin, Scott C. Chapman, Matthieu Béthermin, Scott C. Chapman, Chenxing Dong (董辰兴贞, Anthony H. Gonzale如, Christopher CHayward , Yashar D.Hezaven, 1000) Sreevani Jaruguta, Katrina C. Litke to Matthew A. Malkan Daniel P. Marrone to Department of AstronomyUniversity of Texas at Austin2515 SpeedwayStop C1400 Austin, TX 78712, USA; spilkerj@gmail.com Department of AstronomyUniversity of Illinois, 1002 West Green StUrbana, IL 61801, USA <sup>3</sup> Núcleo de Astronomía de la Facultad de Ingeniería y Cien**das**iversidad Diego Portales.v. Ejército Libertador 441 Santiago Chile Aix Marseille Univ., CNRS, CNES, LAM, Marseille, France <sup>5</sup> Department of Physics and Astronom**y**niversity of British Columbia,6225 Agricultural Rd.,Vancouver,V6T 1Z1, Canada National Research Councillerzberg Astronomy and Astrophysics071 West Saanich RdVictoria, V9E 2E7, Canada Department of Physics and Atmospheric ScienDaJhousie UniversityHalifax, Nova Scotia,Canada 8 Department of Astronomy University of Florida, 211 Bryant Space Sciences Cente ainesville, FL 32611, USA Center for Computational Astrophysics, Flatiron Institute, 162 Fifth Avenue, New York, NY 10010, USA Département de Physiquelniversité de MontréalMontreal, Quebec, H3T 1J4, Canada 11 Steward ObservatoryUniversity of Arizona,933 North Cherry AvenueTucson,AZ 85721, USA <sup>12</sup>Department of Physics and Astronomyniversity of California,Los Angeles,CA 90095-1547,USA <sup>13</sup> University of Florida Informatics Institute 132 Newell Drive, CISE Bldg E251, Gainesville, FL 32611, USA 14 Cosmic Dawn Center (DAWN)DTU-Space,Technical University of Denmark Department of Physics Iniversity of Illinois, 1110 West Green St.J.rbana,IL 61801, USA <sup>16</sup>National Center for Supercomputing Applicationts niversity of Illinois, 1205 West Clark St. Urbana,IL 61801, USA Max-Planck-Institut für Radioastronomiauf dem Hügel 69,D-53121 Bonn,Germany Received 2020 August 25; revised 2020 October 13; accepted 2020 October 22; published 2020 December 16

## Abstract

Massive galaxy-scale outflows of gas are one of the most commonly invoked mechanisms to regulate the growth and evolution of galaxies throughout the universe. While the gas in outflows spans a large range of temperatures and densities the cold molecular phase is of particular interesteause molecular outflows may be capable of suppressing star formation in galaxies by removing the star-forming Wes have conducted the first survey of molecular outflows at z > targeting 11 strongly lensed dusty.star-forming galaxies(DSFGs) with highresolution Atacama Large Millimeter/submillimeter Array observations of OH 119 µm absorption as an outflow tracer. In this first paper, we give an overview of the survey, focusing on the detection rate and structure of molecular outflows We find unambiguous evidence for outflows in 8/11 galaxies (73%) pre than tripling the number known at z□>□4his implies that molecular winds in z□>□4 DSFGsaust have both a near-unity occurrence rate and large opening angles to be detectable in absorption. Lensing reconstructions reveal that 500 pc scale clumpy structures in the outflows are common individual clumps are not directly resolved but from optical depth arguments we expetithat future observations willrequire 50-200 pc spatialesolution to resolve them. We do not detect high-velocity [Qi] wings in any of the sources with clear OH outflows indicating that [C II] is not a reliable tracer of molecular outflows. Our results represent a first step toward characterizing molecular outflows at z \( > \subseteq 4 \) the population level, demonstrating that arge-scale outflows are ubiquitous among early massive dusty galaxies.

Unified Astronomy Thesaurus concepts: High-redshift galaxies (734); Galactic winds (572); Gravitational lensing (670); Galaxy formation (595)

# 1. Introduction

Galactic feedback is now widely recognized as a key componentin our modern understanding of galaxy formation and evolution. "Feedback" is an umbrella term for a wide range 2015), including in massive dusty galaxies athigh redshifts of physical processes enabling self-regulated galaxy growth, setting the efficiency of star formation and shaping fundamental correlations between galaxy properties such as stellar mass, metallicity, star formation rate (SFR), and supermassive black hole mass. One of the most striking observational windows into galactic feedback is the ubiquitous detection of massive outflows of gas and dust being launched from galaxiesvinds). generally thought to be powered by supernovaeand/or supermassive black hole accretiorOutflows of ionized and

neutral atomic gas have been detected in galaxies over a wide range of mass and redshiftor decades (e.g.Heckman etal. 1990; Rupke etal. 2005; Weiner etal. 2009; Chisholm etal. (e.g., Banerji et al. 2011; Casey et al. 2017; Schechter& Casev 2018) More recently observations that robe the cold molecular gas in outflows have been a focus of recent interest because molecular gas is the direct fuel for future star formation and is often the dominantphase in the outflow mass budget (see Veilleux etal. 2020 for a recentreview of cold galactic

In the high-redshift universe, spatially resolved studies of massive quenching galaxies at  $z \square \square \square 2$  typically find evidence for an inside-out suppression of star formation (e.g., Tacchella et al. 2015, 2018; Nelson et al. 2016; Spilker et al. 2019)

<sup>18</sup> NHFP Hubble Fellow.

accompanying a sharp overable crease in the moleculagas fraction compared to equally massive star-forming galaxies at tracers reveathe impact of the wind from the active galactic Tadaki et al. 2017; Talia et al. 2018). Indeed, massive  $(M_{stat}\Box \sim \Box^{1/1}0M_e)$  quiescentgalaxies have been identified in sizable numbers as early as z□~□4 (e.g., Straatman et al. 2014\$uch detailed views of molecular outflows have thus far Guarnieri et al. 2019; Carnall et al. 2020; Valentino et al. 2020), implying a very rapid formation history with SFRs of hundreds of M<sub>e</sub> yr<sup>-1</sup> and subsequentapid quenching of star formation (e.g., Glazebrook et al. 2017; Estrada-Carpenter et allhe faint CO line wings associated with outflows requires 2020; Forrest et al. 2020). The required high SFRs are generally only found in very infrared-luminous systems, in which the UV radiation from young stars is absorbed and reprocessed by dust. These observation paint an appealing picture in which initially gas-rich, dusty, star-forming galaxies (DSFGs) atleast temporarily suppress statormation via the consumption, heating, and/or ejection of the molecular gas fue □>□4 have molecular outflows reported (Spilk al. 2018; to create the early passive galaxy population (elgarayanan

galactic winds in both the nearby and distant universeither of which is easily detectable carbon monoxide (CO) and the hydroxyl molecule OH (e.g., Veilleux et al. 2020). Low-order transitions of CO can be used to detect cold molecular outflowshosts (Weiß et al. 2012; George et al. 2014; Feruglio et al. just as they are often used to probe the overall molecular contents of galaxies more generally (e.g.Valter et al. 2002; Alatalo et al. 2011; Barcos-Muñoz et al. 2018). For unresolved because the emergence of nolecular winds with properties observations, the outflow signature is an excess of CO emission in those observed in real galaxies has proven to be at high velocities relative to systemic that is not plausibly related to rotational or non-rotational motions within the galaxies. CO observations have the benefit of sensitivity to gasvelocities of hundreds of km s

through directram pressure wings are very faint and the geometry of the emitting gas is difficult to constrain (for example, it is hard to distinguish outflowing from inflowing gas because the line-of-sight location of the emission is unknown, or to rule out that the emission is from a separate galaxy in a merger that may not be alternative is that molecules in outflows re-form at apparenteven in deep imaging data). An alternative is farinfrared transitions of OH, demonstrated to be a very good tracer of outflowing and inflowing gas in dozens of nearby galaxies over the lifetime of the Hersche Space Observatory (e.g., Sturm et al. 2011; Spoon et al. 2013; Veilleux et al. 2013, the details of the simulation and the outflow energetics his Stone etal. 2016: González-Alfonso etal. 2017). In this case the outflow (or inflow) signature takesthe form of broad blueshifted (redshifted)absorption profiles against the continuum emission of the host galaxies. Because the gas flows affect constraints on the occurrence structure, and physical seen in absorption, the geometrical interpretation of the line profiles is simplified, but OH studies consequently require to outflowing material that does not intersect the line of sight toreported the highest-redshiftetection of a molecular outflow the hosts.

In the best-studied examples the local universe, the allowing for detailed pictures of the locationkinematics, and conditions within the molecular gas contained in the outflows. still not representative of the general population of high-The prototypical starburst-driven outflows in M82 and NGC 253, for example, are both seen nearly edge-on, and both showboward constraining the occurrence and properties of more out of the disks (e.g., Walter et al. 2002, 2017; Leroy et al. 2015; Krieger et al. 2019). Meanwhile, very highresolution observations of the outflow from the nuclear region presentour new ALMA data. We focus here on the broad

of the nearby Seyfert galaxy NGC 1068 in multiple molecular the same epoch (e.g., Spilker et al. 2016a; Popping et al. 2017 nucleus (AGN) on the surrounding torus, also likely extending to larger spatialscales in the host galaxy (e.gGarcía-Burillo et al. 2019).

been confined to the local univers@espite a handfubf past successesmerely detecting molecular outflows in the early universe at all continues to be extremely challenging: detecting substantialobservationalnyestments even with the Atacama Large Millimeter/submillimeter Array (ALMA) and is generally only possible out to  $z \square \sim \square 2$  except in extreme canses, the detection of OH absorption requires bright continuum fluxes that limit the plausible target galaxies to very IRluminous QSOs and DSFGs. Thus far only three objects at through a self-regulating feedback process or processes in ordeones et al. 2019; Herrera-Camus et al. 2020), and even in these cases the interpretation of the observations is notecessarily clear-cutgiven limitations in signal-to-noise ratio (S/N) and There are two primary tracers of the cold molecular phase of the complex galactic dynamics at play in the early universe. All outflows detected and while selected in very heterogeneous ways, all are limited to luminous dusty galaxies and/or AGN

2017; Fan et al 2018; Herrera-Camus et al 2019). The structure of molecular outflows is of special interest especially challenging for hydrodynamical simulations. In particular, accelerating moleculargas initially at rest up to at all distances and lines of sight to the host galaxy, but the linerom a hot, fast wind or through entrainment in such a wind has proven extremely difficult. The cold and dense gas is shredded by hydrodynamicalinstabilities long before itreaches speeds like those observed in realgalaxies (e.g., Klein et al. 1994; Scannapieco2013; Schneider & Robertson 2017). One large galactocentric distances, cooling out of a hotter wind fluid having already reached velocities those observed (e.g., Zubovas & King 2014; McCourt et al. 2018; Richings & Faucher-Giguère 2018schneider etal. 2018). Depending on cold gas can show either kiloparsec-scale clumpy structures or a fine mist-like morphology on very small scales.

This is the first in a series of papers in which we present the properties of molecular outflows in a sample of DSFGs at  $z\Box>\Box 4$  targeting the OH 119 µm dou**bles** sample expands galaxies with bright continuum emission, and are not sensitive on our work in Spilker et al. (2018, hereafter S18), in which we toward a z□=□5.3 galaXlytargets are gravitationally lensed by foreground galaxies, which allows us to spatially resolve geometry and structure of the winds can be spatially resolved, both the rest-frame 120 µm dust continuum emission as well as the OH absorption at systemic and blueshifted velocities. While redshift galaxies, our goal with this survey is to take a first step clumpy streamers of molecular gas extending a kiloparsec or molecular outflows in the early universe in a statistical sense at the population level.

In this work we give an overview of the sample objects and

sample properties putflow detection rates, and the resolved structure of the molecular outflows we determine from gravitational lensing reconstructions of the sources. In a companion paper (Spilker et l. 2020, hereafter Paper II) we characterize the physical roperties of the molecular outflows we detect focusing on the outflow ratesenergetics and wind objects, ALMA observations, and ancillary data for our objects were estimated using the available far-IR photometrywhich and literature comparison samplesSection 3 describesour analysis methods for the OH spectra, how we classify whether energy distributions (SEDsSection 2.3). We finally required or not objects show signs of outflowand our lens modeling methodology and tests. Section 4 gives our main observationalbservations (Spilker et al. 2016b) and chose objects to span flat  $\Lambda$ CDM cosmology with  $\Omega_{\rm m}\Box = \Box 0.30\bar{a}$  nd  $H_0\Box = \Box 67.7$ km s<sup>-1</sup> Mpc<sup>-1</sup> (Planck Collaboration et al. 2016), and we take the total infrared and far-infrared luminosities IR and LFIR to be integrated over rest-frame 8-1000 and 40-120 µm, respectively. Tables of the sample properties from this work, as extremely luminous objects  $\phi(L_{|R}/L_{|}) = 12.5-13.5$ ; they well as the outflow properties from Paper Ilare available in electronic form at https://github.com/spt-smg/publicdata.

# 2. Sample and Observations

# 2.1. Parent Sample and Source Selection

We designed an observing campaign targetin ΩH <sup>2</sup>Π<sub>3/2</sub> J□= $\square 3/2\square \rightarrow \square 5/2$  absorption. This transition is a  $\land$  doublet with components at est-frame 2509.9 and 2514.3 GHz (separated by  $\sim$ 520 km  $\rm s^{-1}$ ) and additional hyperfine structure that remains spectrally unresolved. We selected source for OH observations from the point-source catalog of the 2500 deg 2011; Mocanu et al. 2013; Everett et al. 2020). From the surveground the OH linesdepending on the redshift of each source. data and subsequents bervations using the APEX/LABOCA camera at 870 µm, a total of 81 objects were selected with spectral indices consistent with thermal dust emission (namelytransition (or ≈680 km s̄¹ redward of the lower-frequency  $S_{1.4 \text{ mm}}/S_{2 \text{ mm}} \square > \square 1.8$  aw 1.4 mm flux density greater than 20 mJy, flux density at 870 µm greaterthan 25 mJy, and no low-redshift interlopers. Given their extreme brightness, the ally lensed by foreground galaxies. High-resolution ALMA imaging confirmed the lensed nature ofthese sourceswith typical magnifications of 3-30 (Hezaveh et al. 2013; Vieira et al. 2013; Spilker et al. 2016b). Extensive spectroscopic campaigns subsequently measured spectroscopic redshifts for the entire sample, which range from 1.87 to 6.90 with a median of 3.9 (Weiß et al. 2013; Strandet et al. 2016; Marrone frequency of the ALMA Band 8 receivers, these continuum et al. 2018; Reuter etal. 2020), although notall sources had known redshifts at the time the presentoutflow survey was designed.

was that the source redshift place the OH doublet lines at frequencies of relatively good atmospheric transmission in ALMA Band 8 (385–500 GHz), requiring z<sub>source</sub>□ □ □ 4.02 (to reach ALMA Band 7 requires₀Grce□>□5.8, where we have few estimated using the available far-IR and (sub)millimeter available targets). The atmospheric transmission at these frequencies is strongly affected by telluric watexygen, and ozone features so OH observations are not feasible for all sources at z□>□4n particular, OH observations are not 

deep atmospheric features. We restricted the sample to sources with redshifts that avoided frequencies of oor transmission, and predicted 119 µm continuum flux densities brightough that ALMA would be able to reach sensitivities of 5% of the continuum level in ~200 km s<sup>1</sup> channels in less than an hour of observing time after resolving the source over 5-20 driving mechanisms. Section 2 gives an overview of the sampleesolution elements These predicted continuum flux densities provides very good sampling of the long-wavelength spectral that all targets have lens models from ALMA 870 µm results, with additional discussion in Section 5. We summarize a wide range in In. The sources selected for OH observations our principal findings and conclude in Section 6. We assume a are not obviously biased with respect to the full SPT sample of z□>□4 DSFGs in intrinsic (lensing-corrected) dust mass, or effective dusttemperature (Reuter et l. 2020), although this remains somewhatncertain because we lack lens models for every SPT DSFGEven after lensing correction these remain are certainly not "typical" galaxies at these redshifts by any conceivable definition.

> The final sample consists of 11 objects  $at 09 \square < \square z \square < \square 5.30$ including SPT2319-55, previously published in \$18. Basic properties of the sample are given in Tables 1 and 2, with a few salient properties shown in Figure 1.

# 2.2. ALMA Observations

ALMA observed our sample galaxies across severajects from 2016 to 2019, summarized in Table 1. For each object, we configured the correlator to observe the OH doubleth two slightly overlapping 1.875 GHz wide basebands and 3.9 MHz SPT survey at 1.4 and 2 mm (Vieira et al. 2010; Carlstrom et abhannels, providing contiguous coverage over 2200–2700 km s These basebands were placed such that the lower-frequency edge correspondedo ≈1200 km s

¹ redward of the upper OH transition), leaving ≈1000–1700 km to the blueshifted side of the upper-frequency doublet transition. This setup was chosen to detection in various shallow multiwavelength surveys to reject maximize the amount of blueshifted velocity coverage while still allowing both doublet transitions to be detected. Unfortunately it vast majority of these sources were expected to be gravitation-does not allow for the detection of strongly redshifted emission (or absorption), as expected for the classical P Cygni profile and sometimes observed in the OH spectra logical ultraluminous infrared galaxies (ULIRGs) and quasar hosts (e.g., Veilleux et al. 2013). We also placed an additional two basebands of 1.875 GHz width each for continuum coverage in the other sideband of the ALMA correlator. Given the fixed 4-8 GHz intermediate measurements re centered either 12 GHz above or 12 GHz below the OH frequencies in Table 1, depending on the atmospheridransmissionFor SPT0459-59 and SPT2132-58 Our primary selection criterion for OH 119 µm observations the atmospheric transmission is poor both above and below the OH observed frequenciesmaking half (SPT0459-59)or all (SPT2132-58) of the continuum bandwidth unusable.

The observing time and requested spatialesolution were photometry and the lens models available from high-resolution ALMA imaging for each individual source (Spilker et al. 2016b; Reuter etal. 2020). The array configuration(s) varied for each source, with maximum baseline lengths ranging from 4.68, 4.86 □ □ □ z □ □ □ 4.99, and 5.43 □ □ □ z □ □ □ 5.53 duedbsæspetidalls. The shortest baselines lead to maximum

Table 1 Summary of ALMA Observations

Source	R.A.	Decl.	v <sub>obs</sub> (GHz)	Program ID	t <sub>obs</sub> (minutes)	Beam Size (arcsec)	σ <sub>cont</sub> (μJy beam̄¹)	<i>S</i> <sub>100 km š</sub> ¹ (mJy beam̄¹)
SPT0202-61	02 <sup>h</sup> 02 <sup>m</sup> 58 <sup>s</sup> 86	- 61021¢110.1	417.8	2016.1.00089.S	43	0.37□×□0.45	64	0.41
SPT0418-47	04 <sup>h</sup> 18 <sup>m</sup> 39§67	- 47051¢520.7	481.2	2015.1.00942.\$	12	0.11□×□0.16	250	1.28
				2018.1.00191.S	87	0.32□×□0.46	110	0.67
SPT0441-46	04 <sup>h</sup> 41 <sup>m</sup> 44 <sup>s</sup> 08	- 46105¢251.5	459.1	2015.1.00942.S	11	0.14□×□0.18	352	2.10
				2016.1.00089.S	17	0.25□×□0.33	205	0.89
				Combined	28	0.22□×□0.30	178	0.84
SPT0459-58	04 <sup>h</sup> 58 <sup>m</sup> 59 <sup>s</sup> 80	- 58105¢141.3	429.4	2019.1.00253.S	40	0.33□×□0.40	82	0.69
SPT0459-59	04 <sup>h</sup> 59 <sup>m</sup> 12 <sup>§</sup> 33	- 59142¢201.6	433.6	2019.1.00253.S	41	0.33□×□0.41	120	0.56
SPT0544-40	05 <sup>h</sup> 44 <sup>m</sup> 00 <sup>s</sup> 80	- 40136¢311. 1	477.2	2019.1.00253.S	32	0.28□×□0.31	103	1.00
SPT2048-55	20 <sup>h</sup> 48 <sup>m</sup> 22 <sup>s</sup> 86	- 55120¢211. 3	493.7	2018.1.00191.S	48	0.37□×□0.44	118	0.72
SPT2103-60	21 <sup>h</sup> 03 <sup>m</sup> 30 <sup>s</sup> 85	- 60132¢401.5	462.6	2016.1.00089.S	23	0.46□×□0.49	238	1.10
SPT2132-58	21 <sup>h</sup> 32 <sup>m</sup> 43 <sup>s</sup> 23	- 58102¢461. 2	435.9	2015.1.00942.S	17	0.32□×□0.50	345	1.64
SPT2311-54	23 <sup>h</sup> 11 <sup>m</sup> 23 <sup>s</sup> 97	- 54150¢301.2	476.2	2015.1.00942.S	45	0.15□×□0.20	157	1.27
				2018.1.00191.S	49	0.28□×□0.37	91	0.92
				Combined	94	0.23□×□0.30	80	0.75
SPT2319-55	23 <sup>h</sup> 19 <sup>m</sup> 21 <sup>s</sup> 67	- 55157¢571.8	399.4	2016.1.00089.S	30	0.27□×□0.39	71	0.52

Notes. All beam sizes and sensitivities are measured from naturally weighted images. The spectral line sepsitivitis measured in a 100 km1schannel near the upper OH rest frequency

<sup>b</sup> Reproduced from Spilker et a(2018).

Table 2 Summary of Sample Properties

Source	Z <sub>lens</sub>	Z <sub>source</sub>	μ	$L_{IR} (10^{12} L_{e})$	$L_{FIR} (10^{12} L_{e})$	f <sub>AGN</sub>	$M_{\rm H_2}  (10^9  {\rm M_e})$	r <sub>cont</sub> (kpc)
SPT0202-61	L	5.0180	17.5	9.6□±□1.5	4.6□±□0.6	<0.25	25.1□±□3.5	0.72
SPT0418-47	0.26	4.2248	37.2	3.0□±□0.5	1.7□±□0.2	<0.1	6.0□±□0.5	0.74
SPT0441-46	0.88	4.4770	11.5	6.1□±□1.3	3.5□±□0.6	<0.15	12.3□±□2.0	0.53
SPT0459-58	L	4.8560	7.3	8.1□±□2.0	4.5□±□0.8	<0.2	27.4□±□3.3	1.22
SPT0459-59	0.94	4.7993	3.1	18.1□±□5.7	9.9□±□2.0	< 0.3	79.9□±□7.0	3.99
SPT0544-40	L	4.2692	10.5	7.3□±□1.1	4.3□±□0.6	<0.2	46.6□±□4.3	0.69
SPT2048-55	L	4.0923	10.8	4.5□±□1.2	2.6□±□0.5	<0.2	16.0□±□2.6	0.67
SPT2103-60	0.76	4.4357	20.9	2.9□±□0.5	1.7□±□0.3	<0.15	9.8□±□1.7	1.02
SPT2132-58	L	4.7677	5.7	11.3□±□4.3	6.2□±□1.4	<0.25	27.6□±□2.6	0.78
SPT2311-54	0.44	4.2795	2.5	29.8□±□7.9	16.2□±□2.9	<0.45	63.5□±□4.9	1.08
SPT2319-55	0.91	5.2943	5.8	7.9□±□3.0	4.3□±□0.8	<0.3	11.8□±□2.1	0.92

Notes. L<sub>R</sub> and L<sub>FIR</sub> are integrated over rest-frame 8–1000 and 40–120 μm, respectively. All values have been corrected for the lensing magnification μ; we estimate uncertainties of ~15% on the magnification of AGN-heated dust to the rest-frame 5-1000 μm luminosity; upper limits 4 με 1σ. from Aravena et al. (2016) and M. Aravena et al. (2020, in preparation) using updated magnifications from this workntrinsic dust continuum sizes  $\xi_{ont}$  are circularized radiiof the regions where the continuum is detected \$\frac{3}{u}\text{N} \subseteq > 15 in the lensing reconstruction residuals is available in machine-readable format https://github.com/spt-smg/publicdata.

The data were reduced with the standard pipelines available folength or half the scan length. This self-calibration was each ALMA cycle, with additional manual calibration and flagging where necessary Besides the typicabandpassflux, and complex gain calibrators, all observing blocks also recorded data for a guasar near each DSFG used as a test frequency and high-resolution ALMA observing Images of these testources showed astrometric shifts of up to ~0."1 and atmospheric decorrelation of up to 30%, evidence or between sidebands). of residual atmospheric phase noise varying fastethan the source-calibrator observing cycle o mitigate this noise, we

recoverable scales ☐2 5 depending on observing frequency; attempted one or two rounds of phase-only self-calibration on we do not expect significant emission on larger spatial scales. the test and target sources, using solution intervals of the scan successfufor all sources excep\$PT2103-60 decreasing the image rms by up to a factor of two. We note that selfcalibration makes absolute astrometry impossible, so the astrometry of these data should be considered accurateto the astrometry and calibration quality; this is standard for high-~0."1, as measured from observations of the test source before self-calibration. Self-calibration has no influence on the relative astrometry within the ALMA data (e.g., across the line profiles

We generate images of each targesing naturalweighting of the visibilities, which maximizes sensitivity athe expense

<sup>&</sup>lt;sup>a</sup> SPT0418-47 was observed in 2015.1.00942.S at much higher spatial resolution than requested. Given the large extent of the source and the short observing dur these data have too low an S/N to be usable and are excluded from all figures and models include the observations in this table for completeness.

<sup>&</sup>lt;sup>a</sup> Excludes the faint source southwest of the lensed source (see Figure 2).

<sup>&</sup>lt;sup>b</sup> Reproduced from Spilker et a(2018).

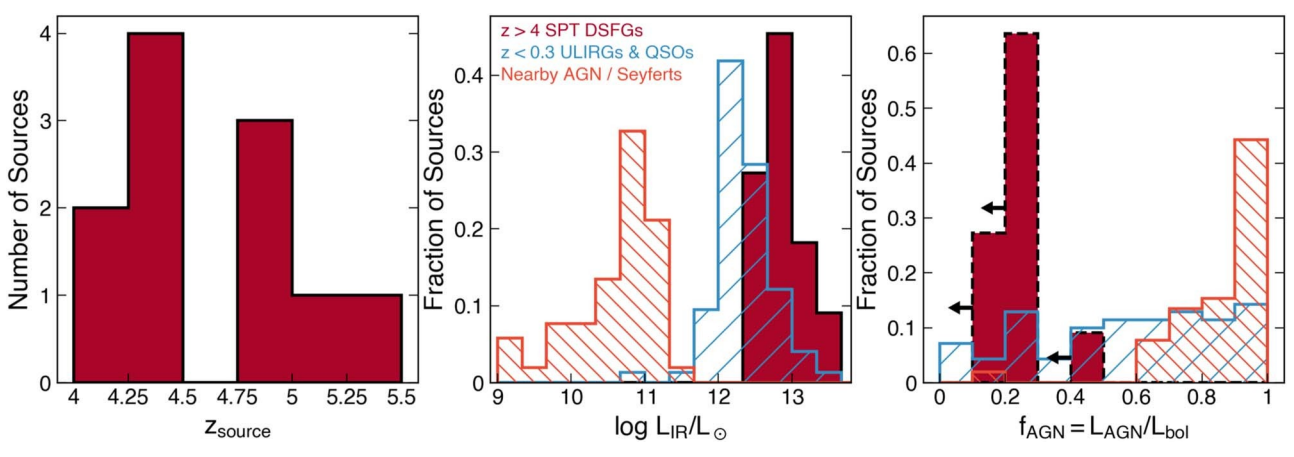


Figure 1. Summary of source properties for our SPT-selected sample of high-redshift DSFG outflows and literature comparison samples detailed in Section 2.4. Al fagn values for the SPT sample are upper limits, although the rest-frame mid-IR data used to computer fail in the event of extremely high column densities hiding highly obscured AGN.

of spatial resolution. Natural weighting is also the closest approximation to the visibility weighting used in our subsequen 2020), correcting for the lensing magnifications of each source visibility-based lens modeling procedure(Section 3.3). We followed standard imaging proceduresmanually applying a clean mask overregions with clear, high-S/N emission, and stopped the image cleaning at five times the image noise level.SPT 1.4, 2, and 3 mm photometry and ALMA 870 µm and Continuum images were created combining allailable data, while image cubes of the OH lines were created with channel between simple modified blackbody fits and more complex resolutions varying from 50 to 150 km in order to maximize the S/N. To extract integrated OH spectra, we performed aperture photometry within the region where the continuum is detected at>3σ. We also performed a similar procedure on image cubes created by tapering the visibilities to resolutions ~2-3 times lower than the fulldata and find no evidence that significant flux has been resolved out in our observations. Continuum images of each source are shown in Figure 2 and integrated spectra in Figure 3.

# 2.3. Ancillary Data

In addition to the ALMA OH observations that are our primary focus, we also use a variety of ancillary photometric and spectroscopicdata to aid in the interpretation of the OH data.

The systemic redshiftand line profile of gas within each galaxy are key to our interpretation of the OH spectification available (five sources)we use very high-S/N ALMA [C II] 158 µm spectra, observed in program 2016.1.01499.S (see While these data have fairly high spatial resolution, \( \frac{1}{2} \)0 3, we use only the integrated [C] line profile extracted similarly to the OH spectra. For those sources without igh-quality [CII] data, we instead stack the spectra of all available transitions oftemperatureratio of 0.9 between the CO(2-1) and (1-0) CO for each sourceweighted by the S/N of each line. These CO lines were observed with ALMA and the Australia TelescopeCompactArray (ATCA), and were the primary features used to measure the redshrifteach source. The CO lines include CO(2-1) and CO(5-4) for all sources and CO(4-3) for z□<□4.4@ach typically detected at S/N ~ 5-10. For the sources with ALMA [CII] spectra, we find no evidence for a difference in line width compared to the CO lines with lower S/N.

We measure the IR  $(8-1000 \mu m)$ and far-IR  $(40-120 \mu m)$ luminosities by fitting to the available far-IR and submillimeter

photometry (Weiß et al. 2013; Strandet et al. 2016; Reuter et al. as described further in Section 3.3. For all sources, the available data include Herschel/PACS and SPIRE data at 100, 160, 250, 350, and 500 μm, APEX/LABOCA 870 μm, the 3 mm data. We find consistent results for the luminosities modeling because the far-IR SED is very wellsampled.We also make use of the PACS photometry at 00 and 160 µm, which probes rest-frame mid-IR wavelengths  $\square \sim 15-30$  tom, constrain the contribution of hot dust heated by AGN activity. We use the CIGALE SED fitting code (Burgarella et al. 2005; Boquien et al. 2019) to place limits on the fractional AGN contribution to the totalluminosity integrated over rest-frame 5–1000 µm f<sub>AGN</sub>; no source shows strong evidence for AGNrelated mid-IR emission. For the low-redshift comparison samples (Section 2.4)it is more common to measure f<sub>AGN</sub> using the rest-frame 30 µm/15 µm flux ratio assuming fixed mid-IR flux ratios for pure star formation and pure AGN emission. While we prefer the CIGALE fitting values for easier comparison with typical practice in the extragalactic literature, we have verified that we recover to within □≈0.2-0.3 using the mid-IR color definition. We note that it is possible that our target galaxies are optically thick at mid-IR wavelengths, which could hide very highly obscured AGN and result in less strict limits on f<sub>AGN</sub> than we adopt here (e.gSnyder et al.2013).

Masses of molecular gas were measured from observations Litke et al. 2019 for a representative object from this sample). of CO(2-1) using ATCA. Five of the 11 sources in our sample were published in Aravena et al. (2016), while the remainder have been observed and analyzed using the same procedures and will be published elsewhere assume a line brightness transitions and a CO-H<sub>2</sub> conversion factor  $\alpha_{CO} \Box = \Box 0.8 \text{ eM}$  $(K \text{ km s}^{-1} \text{ pc}^2)^{-1}$ , both typical for highly star-forming DSFGs like our sample (Spilker et al. 2014, 2015; Aravena et al. 2016).

# 2.4. Literature Comparison Samples

Throughout this work we compare to a number of studies of OH absorption in low-redshift galaxies performed by the Herschel/PACS instrument/While detailed sensitivity metrics (e.g., the typical fractional contrast compared to the continuum reached perspectral element) are generally not given, the

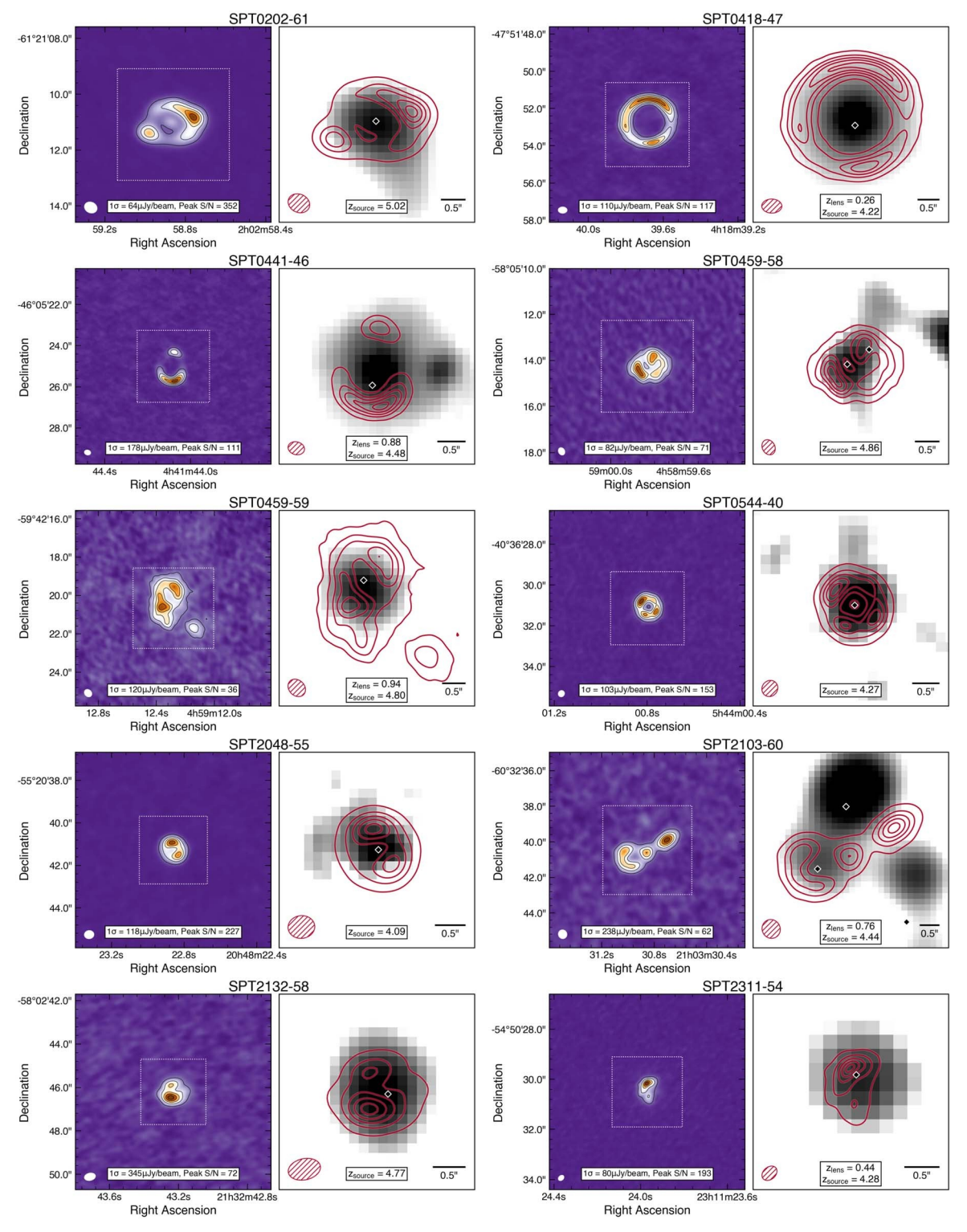


Figure 2. Left: □rest-frame 119 µm ALMA continuum images of each sample object. Contours are drawn at 10%, 30%, 50%, 70%, and 90% of the peak. Squares r the zoomed regions in the rightpanels. Right: ALMA continuum contours overlaid on the bestvailable near-IR images from severdifferent facilities (Spilker et al. 2016b), which detect only the foreground lensing galaxies. Diamonds mark the best-fit positions of the lens(es); we do not use these images to constrain the positions because the astrometry is more uncertain than the uncertainties on the positionsses at lower left show the synthesized beam.

published spectra of these source appear to be of broadly similar quality to our own. A brief description of these samples the SHINING key program (Sturm et al. 2011) with 15 follows, and a few relevant quantities are summarized in Figure 1.

Veilleux et al. (2013) presentOH spectra of 43 nearby galaxy mergers, mainly consisting of ULIRGs and IR-luminous from the HERUS program (Farrah et al. 2013) that largely

QSOs. The sample supplements 23 galaxies observed as part of additional sources selected to have higher values of and a further five chosen to be less IR-luminous than the full sample. Spoon et al. (2013) present an analogous sample of 24 ULIRGs

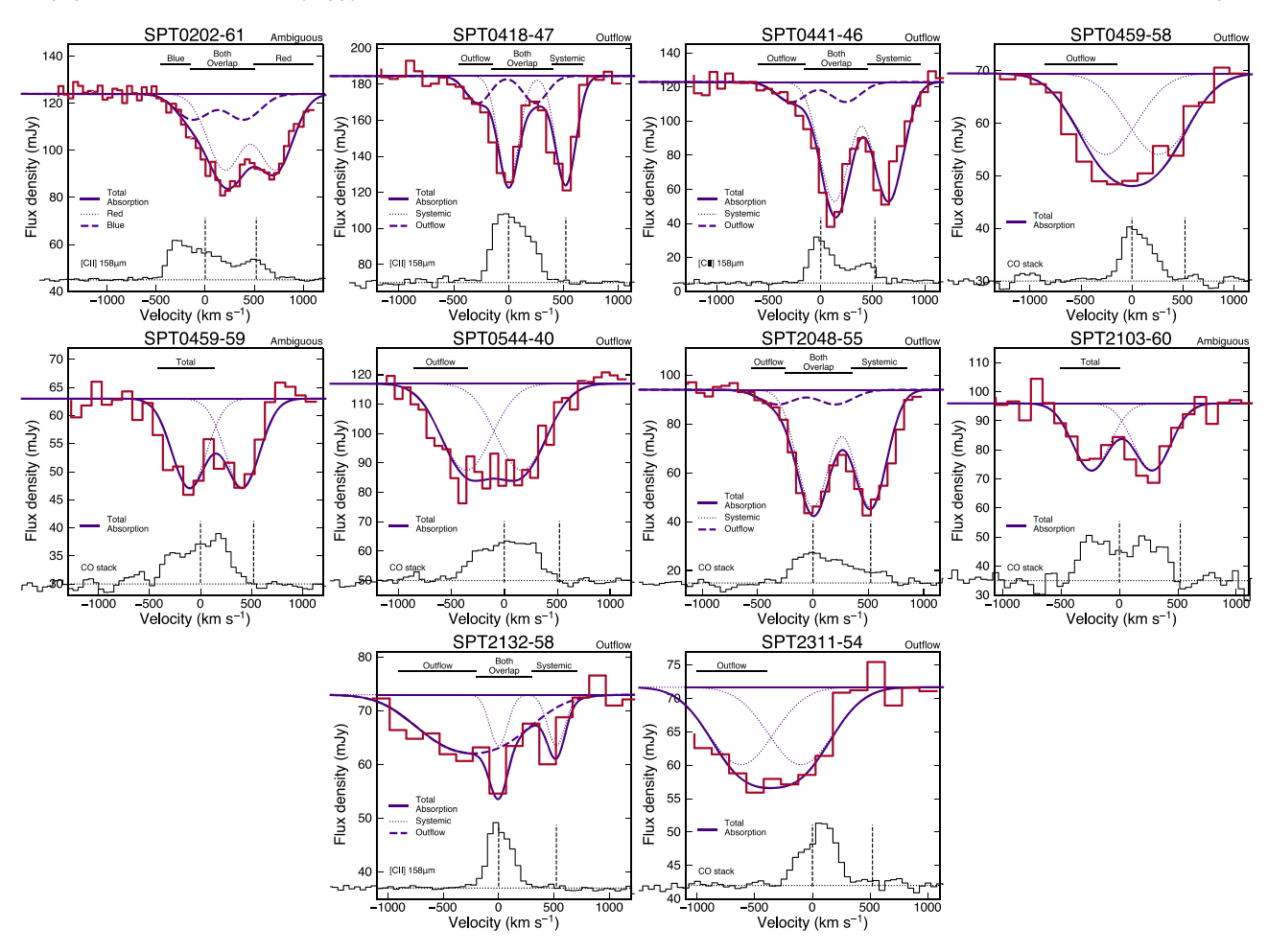


Figure 3. OH 119 µm spectra of each sample target (red), not corrected for lensing magnification. Also overplotted are fits to the spectra using either one or two pa of Gaussians (navy lines), as detailed in Section 3.1. Vertical dashed lines show the rest velocities of the two OH doublet components, where we assign the higher frequency transition to zero relative velocity help interpret the complex OH doublet spection also show a "reference" line profile of [0] or CO, which is expected to be dominated by gas internal to the galaxies. Horizontal bars at top label the velocity ranges we selected for lens modeling, chosen to be dominated b single velocity components (we also label the velocity ranges where multiple velocity components overlap, where applicable). There is clearly a large diversity of lin profile shapes, but at least 7/10 of these sources host molecular outflows as defined by absorbing components more blueshifted than the reference line emission. remaining three sources typically show broad reference line profiles with multiple peaks themselving interpretation of the OH line profiles difficult.

overlap in source properties. Calderón et al. (2016) and Herrera-Camus eal. (2020) further expand on the aforementioned samples, presenting a combined total of nine ULIRGs atfound results consistent with the published values. slightly higher redshifts (z - 20.25) and correspondingly higher A handful of additional high-redshift objects besidesour typical luminosity (og( $L_{\rm IR}/L_{\rm II}$ )  $\sim$  12.5-13.5) to ensure sufficiently bright continuum fluxesWe collectively refer to these samples as "ULIRGs and QSOs" throughout this work.

Stone et al.(2016) present OH observations of a sample of 52 nearby hard X-ray-selected AGN. These sources are the least similar to the other samples or to the  $z\Box > \Box 4$  SPT DSFGsata, and is outflowing with respect to that clump. Those consisting of objects more than an orderof magnitude less luminous  $(L_R \square \square \square 1 1 D_e)$  than those in the other samples but whose bolometric luminosities are dominated by the AGN power (typically  $f_{AGN} \square > \square 0.80$ ) ver half of this sample shows OH only in emission, a common feature among AGNdominated systems and only 17 show OH in absorption. which Stone et aluse to define their outflow detection rate.

For these low-redshift samples, we adopt the sample properties as published by the original uthors. Although for maximal consistency we would remeasure or example, LIR and fAGN using the same methods as for our own samplee prefer the literature values becausethey are publicly and

centrally available. We spot-checked a few sources from the various samples using far-IR photometry from the literature and

sample have published OH 119 µm spectra. George et al. (2014) presenOH data for SMM J2135-0102 (the "Eyelash" DSFG) at  $z \square = \square 2.3$ . Those authors argue that the OH absorption is associated with one of several spatio-kinematic "clumps" seen in the dust continuum emission in early interferometric clumps have recently been shown to be false (Ivison etal. 2020), so it is unclear how to interpret the OH spectrum in light of the new understanding of the source structure. By our adopted definition (Section 3.2) this source would not be classified as an outflow because the absorption is fully contained within the cores of the bright CO and I@mission lines. Additionally, Herrera-Camus et al. (2020) present ALMA spectroscopy of a  $z\square = \square 6.1$  quasar with a tentative  $3\sigma\square$  detection of blueshifted OH absorption. Given the tentative nature of this detection we also consider this case to be inconclusive. Finally, Zhang et al. (2018) detect OH 119 µm in a stack of 45 lensed DSFGs at  $1 \square < \square z \square < \square 3.6$  and  $\sim 3\sigma$  detections in two individual

objects, but the spectral resolution was too low to measure anylensing reconstructions to measure the structure of the velocity shifts or search for blueshifted line wings.

## 3. Analysis

# 3.1. Spectral Analysis

While OH is clearly detected in absorption toward each source, the integrated spectra in Figure 3 show a diverse rangerofile. For sources with single broad absorption profiles of absorption depths and line profiles. In about half the sample use the fits to try to avoid double-counting gas at the same the OH doublet lines are sufficiently narrow to be individually resolved, while in the rest they are wide enough to be blended, cases, we prefer to define the outflows as beginning at the creating a single wide absorption profil@ome sources show obvious signs of multiple velocity components contributing to the overall line profile (e.g., SPT0418-47), while others are adequately fit by a single velocity component (e.g., SPT0459-58).

To help interpret these line profiles, we fit the integrated spectra with one or two pairs of Gaussians depending on the complexity of the line profile for each source. These fits are by no means unique, but they do capture the information available The wide diversity in OH absorption profiles among our in the spectra As a Λ doublet, the two 119 μm OH lines are expected to have equal amplitude, and to have a fixed separation in velocity of ≈520 km s<sup>-1</sup>. The free parameters are the continuum flux density and eitheone or two of the absorption depththe velocity offset relative to the systemic, and the Gaussian line width.

We assume a constant ontinuum flux density across the relatively narrow bandwidth of these observations. In a handfulVeilleux et al. 2013; Herrera-Camus et al. 2020). For a variety of sources there are few absorption-free channels to constrain of reasons we find this definition unsatisfying for our sample. absorption that extends out to and beyond the edge of the bander double-peaked [0] or CO lines that are hundreds of kith s (e.g., SPT2311-54). For these sources we also make use of the wide, which makes the redshift used to define systemic (zero) continuum data in the alternate sideband offie ALMA data and/or a global fit to the long-wavelength SED.Rest-frame 119 µm is near the peak of the dus&ED where the slope is nearly flat, and we estimate thattaking the continuum level a few per cent in the continuum level of the OH sideband due the total absorption profiles are often a superposition of a to the sideband wavelength separation. We tested this procedure using the sources with sufficient line-free bandwidthcomponentwith a typically much weaker absorption depth. in both sidebands and find no appreciable differences in the Off here is no reason to expedit at the presence or strength of fit parameters.

We derive several other parameters from the best-fit Gaussian profiles. The OH equivalent width is straightforward to derive from the fitting results. We also report several velocity-related quantities to facilitate comparison with literature samples, including and v64, the velocities above which 50% or 84% of the absorption takes place, and  $V_{\text{max}}$ , the estimated terminabutflow velocity. As in \$18, here we take  $V_{\text{max}}$  to be the velocity above which 98% of the absorption occurs. Various definitions of  $V_{\text{max}}$  have been used in the literature, and its value depends on the S/N of the data (and, formethod can change the facthat a source shows absorption SPT2311-54the assumption thathe absorption continues to follow a Gaussian profile beyond the edge of the ALMA bandwidth). We note that these fit parameters are largely immune to gravitational lensing, since both the continuum and outflow classification based on v<sub>50</sub>). It may also exclude absorption musbe magnified by nearly the same factor.he line profile best-fit and derived parameters are given in Tables &O. However, studies of local objects in multiple outflow and 4.

Finally, we use the fits to the OH line profiles and the ancillary spectrabata to define velocity ranges dominated by either outflowing or systemic absorption that we later use in oupur sources. In such cases additional information (such as

absorbing components the wide variety of OH line profiles makes it difficult to define these ranges with unambiguous criteria, and we have no way to separatelow-velocity outflowing materialfrom high-velocity systemic materia.For sources with multiple velocity components, we take the systemic and outflowing components to be those velocity ranges where each componedominates the totalbsorption source-frame velocity due to the Λ doublesplitting. In both velocity where we no longer detect CO or IC emission, but this is not always possible given the relatively weak absorption seen in some sources. In total, we are confident that the velocity ranges we select are at least dominated by outflowing or systemic gasalthough in some cases not exclusively so.

## 3.2. Molecular Outflow Classification

sample raises the obvious question of how to determine whetheror not a particular source has a molecula outflow. Various definitions to answer this question have been used in the literature. Perhaps the most common method is to classify any source with  $y_0 \square < \square -50 \text{ km}^1 \text{sas an outflow,as done by}$ Rupke et al. (2005) and subsequently adopted by several studies of OH in low-redshift galaxies with Herschel (e.g.,

the continuum level (e.g., SPT0544-40), or there is blueshifted First, it is clear that many of our sources have very broad and/ velocity somewhat arbitrary. In other words, the relevant metric is not whether the absorption appears to be blueshifted based on the assigned systemic velocity, but whether the absorption is blueshifted relative to the emission line profiles of the gas from the alternate sideband introduces an uncertainty of at mostithin the galaxies. Second, this definition ignores the fact that componentat systemic velocities and a second blueshifted absorption at systemic velocities has any bearing on whether or not an outflowing component is also present. Objects with extremely deep systemic absorption (e. \$PT0441-46) have v<sub>50</sub> biased by this very strong systemic absorption singeis measured from the total absorption profile.

> Instead, we define a source as containing an outflow ifit shows OH absorption more blueshifted than the detected [C or CO emission, which we expect to be a conservative definition. The benefit of this definition is that outflows defined this way are unambiguous—no fitting technique oranalysis blueshifted more than any gas in the host galaxy. This definition has the drawback of being dependent on S/N, which may exclude weak outflows (although this is also true of sources in which the outflow shows strong emission in [60] tracers typically find that the high-velocity emission outside the line cores is indeed very weak (Lutz etl. 2020), and we see no evidence for high-velocity wings of emission in any of

Table 3
Spectral Fitting Results and Lens Model Velocity Ranges

Source	S <sub>119 µm</sub> (mJy)	Component	V <sub>cen</sub> (km s <sup>-1</sup> )	S <sub>abs</sub> (mJy)	FWHM (km s <sup>-1</sup> )	Eq. Width (km s <sup>-1</sup> )	Model v <sub>cen</sub> (km s <sup>-1</sup> )	Model Δv (km s <sup>-1</sup> )
SPT0202-61	124.4□±□0.6	Red	+200□±□30	-31.7□±□2.9	410□±□50	120□±□9	+800	600
		Blue	-130□±□80	-10.9□±□2.8	400□±□120	34□±□9	-300	300
SPT0418-47	184.4□±□1.2	Systemic	0	-58.8□±□2.7	220□±□20	83□±□8	+535	270
		Outflow	-280□±□30	-14.8□±□2.9	260□±□90	18□±□5	-300	300
SPT0441-46	123.0□±□1.5	Systemic	+130□±□10	-68.0□±□2.8	330□±□30	197□±□20	+700	500
		Outflow	-280□±□80	-11.7□±□2.6	350□±□160	38□±□10	-375	450
SPT0459-58	69.6□±□1.1	Outflow	-260□±□20	-15.4□±□1.3	730□±□120	176□±□22	-500	700
SPT0459-59	63.0□±□0.6	Total	-110□±□20	-15.8□±□1.3	400□±□30	107□±□8	-145	550
SPT0544-40	116.9□±□1.5	Outflow	-360□±□20	-29.4□±□2.5	560□±□60	165□±□27	-600	500
SPT2048-55	94.0□±□1.3	Systemic	0	-48.3□±□2.2	340□±□20	213□±□8	+600	500
		Outflow	-320□±□50	-6.1□±□3.2	380□±□160	26□±□5	-400	300
SPT2103-60	96.2□±□1.2	Total	-240□±□20	-23.6□±□2.2	380□±□30	97□±□7	-250	500
SPT2132-58	73.1□±□1.9	Systemic	0	-9.5□±□3.0	190□±□40	19□±□7	+500	400
		Outflow	-490□±□70	-7.7□±□1.6	750□±□320	99□±□23	-550	700
SPT2311-54	71.7□±□1.2	Outflow	-620□±□40	-11.6□±□1.9	660□±□160	118□±□12	-700	600
SPT2319-55	52.1□±□0.5	Systemic	0	-7.8□±□1.2	330□±□80	52□±□15	+500	400
		Outflow	-440□±□50	<b>-</b> 7.0□±□1.2	450□±□60	64□±□14	<b>-</b> 450	500

Notes.OH spectral componerfts are labeled as in Figure 3Velocities are relative to the higher-frequency OH doubletnsition. Systemic profiles centered on 0 km s<sup>-1</sup> were fixed to the systemic redshift of those sources. Equivalent widths are given for only one of the OH doublet transitions (i.e., they should be multiplied to 2 for the total equivalent width). The final two columns give the center velocity and width that we use for lens modeling, selected to be dominated by each absorbing component (see Figure 3).

Table 4
OH Absorption Profile Characteristics

Source	Outflow?	v <sub>50</sub> (km s <sup>-1</sup> )	V <sub>84</sub> (km s <sup>-1</sup> )	V <sub>max</sub> (km s 1)
SPT0202-61	L	+135□±□10	-115□±□25	-370□±□55
SPT0418-47	Υ	-35□±□10	-230□±□50	-430□±□80
SPT0441-46	Υ	+100□±□10	-120□±□45	-440□±□75
SPT0459-58	Υ	-260□±□20	-560□±□60	-890□±□100
SPT0459-59	L	-110□±□20	-280□±□25	-460□±□40
SPT0544-40	Υ	-360□±□20	-590□±□90	-830□±□170
SPT2048-55	Υ	-25□±□10	-210□±□30	-480□±□85
SPT2103-60	L	-240□±□20	-400□±□20	-570□±□30
SPT2132-58	Υ	-360□±□60	-750□±□120	-1110□±□220
SPT2311-54	Υ	-620□±□35	-900□±□65	-1200□±□ <b>f</b> 05
SPT2319-55	Υ	-215□±□40	-525□±□40	-760□±□60

Notes. See Section 3.2 for our metrics for whether or not a given source shows is indicative of an outflow. We note that using an alternative outflow definition, velocities above which 50%, 84%, and 98% of the total absorption takes place,  $V_{50} \square < \square -50$  km s would still result in 7/11 sources being see Section 3.1.

kinematics at high spatial resolution) would be needed to systemic), which results in a biased value of Non the other determine whether the bright emission is associated with gas inhand, the two sources that would be classified as outflows the host galaxy, a merging partner, or a bona fide outflow. With based on the  $y_0$  criterion, but which we label as ambiguous, this classification we consider 8/11 sources in our sample to are sources with broad CO emission, where the OH absorption show unambiguous signs of molecular outflow (detailed further profile is still fully contained within the brightemission from gas inside the galaxies. The OH could simply be absorption

Compared to some literature classifications,our outflow detection rate could be considered a conservative limit. In particular at high redshift we would call the outflows in the z $\square$ = $\square$ 6.1 quasdLAS $\square$ J1319 $\square$ + $\square$ 0950 (Herrera-Catnals 2020), the z $\square$ = $\square$ 2.3 DSFG SMM $\square$ J2135-0102 (Georgal. et 2014), and the z $\square$ = $\square$ 5.7 DSFG SPT0346-52 (Jones et al. 2019) ambiguous cases instead of confirmed outflows. In the first case the OH spectrum has too low an S/N to be confidentin its classification (and was also noted as tentative by those authors), while in the latter two cases the absorption lines used to claim outflow are fully contained within the bright [ $\square$ ] line profile cores.In the case of SPT0346-52,itke et al. (2019) suggest that the galaxy is actually a major merger based on modeling of the [ $\square$ 1] data. The absorption is well aligned with one of the [ $\square$ 1] line peaks and is instead mostlikely simply systemic absorption within one of the merging pair. This particular object highlights that in such cases kinematics attigh spatial resolution can clarify whether or not a given absorption profile

We note that using an alternative outflow definition,  $v_0v_0\Box < \Box -50 \text{ km}^3 \text{s}$ , would still result in 7/11 sources being classified as showing outflows, with five sources exhibiting outflows both by this metric and by our preferred definition. The three sources that we identify as showing outflows but with  $v_0\Box \Box -50 \text{ km}^3$ , as expected, all have very strong absorption at systemic velocities (or even slightly redshifted from systemic), which results in a biased value  $v_0$ . On the other mand, the two sources that would be classified as outflows thased on the  $v_0$  criterion, but which we label as ambiguous, are sources with broad CO emission, where the OH absorption rprofile is still fully contained within the brightemission from gas inside the galaxies. The OH could simply be absorption internal to the galaxies, and we are not confidentenough to label them outflows despite their  $v_0$  values. This comparison highlights the value of having high-quality reference emission

<sup>&</sup>lt;sup>a</sup> Reproduced from Spilker et a(2018).

<sup>&</sup>lt;sup>a</sup> For SPT2311-54 the giveY<sub>max</sub> is an extrapolation of our fit to the spectrum becausethe absorption profile continues beyond the end of the ALMA bandwidth

line spectra and the peril of accepting the results of OH spectral fitting in the absence of additional information.

# 3.3. Lens Modeling Methods and Tests

We create gravitational lens models to reconstruct the intrinsic structure of each source utilizing the pixellated modeling code described in detailn Hezaveh et al. (2016), as in \$18. For each source we fitto the available continuum data, consisting of the data in the line-free sideband of the ALMA data. For SPT2132-58, which has no useful alternate sideband data due to atmospheric opacitye instead simply use the full OH-containing sideband. Once the best-fit parametersof the lensing potential have been determined following the above procedure, we then use these parameters influence the lensing potentiabut our models do not require the inclusion of a second lens to reproduce the data. reconstructhe OH absorption components using the velocity ranges shown in Figure 3 and listed in Table In principle a joint fit to the continuum and absorption components would provide the optimal constraints on the lens model arameters, but this becomes computationally expensive due to the large number of visibilities.

Briefly, the code fits directly to the interferometric visibilities, which we average temporally unless doing so would cause a binned visibility to span more than 10 m in the uv plane. While the code also has the ability to marginalize over residual time-variable antenna-based phasealibration errors, we neglect this capability for computational efficiency. data reduction largely supplants the need fofurther control over the antenna phases. We fit for the lensing potential using models where the peak negative pixels in the source Markov Chain Monte Carlo (MCMC) sampling algorithmn practice, we first use a code that represents the source plane with one or more simple parametric light profiles (Spilker et al. 2016b) to get a reliable estimate of the lens parameters before resolution of the source reconstructionst is not straightforrefitting with the pixellated code in order to minimize the number of MCMC iterations required for the chains to converge.

The lensing potentials described by one or more singular isothermalellipsoid (SIE) mass profiles (e.g.Kormann et al. 1994). Each SIE potential is described by two positional coordinates a strength related to the lensing massand two we allow for additional angular structure in the lensing potential with external shear and low-order multipoles in the main lens (up to m = 4), as parameterized in Hezaveh etl. (2016). The bestfit lens model parameters are given in the Appendix.

The source plane is represented by a grid of pixels that regularized by a linear gradient prior on the source, which minimizes pixel-to-pixel variations in the source plane in order to avoid over- or underfitting the data (Warren & Dye 2003; the regularization is determined by maximizing the Bayesian evidence given a fixed set of parameters for the lensing potential. Because the regularization strength is only for a fixed set of lens parameters, we perform an iterative process of econstruction. We also measure the differences between the fitting for the regularization strength, MCMC fitting for the lens input and best-fitpositions of the artifcial sources, which are parameters, and refitting for the regularization strength until all small in all cases except when the input source lies very near parameters have converged.

# 3.3.1. Model Selection and Tests

We generally begin each modeling process assuming a simple lens potential parameterization adding complexity where necessar@ur models begin under the assumption that the lensing potentiaban be described adequately by a single SIE profile and an external shear component. If this model does not satisfactorily reproduce the dataye introduce additional complexity as needed of SPT0459-58 and SPT2103-60 he morphology of the lensed images is clearly inconsistent with a simple SIE mass profile, in agreement with the near-IR imaging that shows multiple plausible lensing galaxies neathe main lens. For these sources, we fit models using two (SPT0459-58) or three (SPT2103-60)lensing galaxies. SPT0441-46 also shows a second object 1" west the main lens that may

We use severametrics to determine whether these simple models are sufficient to capture the information in the data or whether further complexity is warranted. We first compare the deviance information criterion of different models (Spiegelhalter et al. 2002), preferring the models with greater likelihood if the additional free parameters from additionalens potential complexity legitimately provide a better fit to the data. Second, in reality we know that the reconstructions of dust continuum emission should be positive but nothing in our methodology forces positivity. If a given model yields a source-plane reconstruction with large negative "bowls," we take this as an indication that the parameterization of the overall lensing In any case, the phase self-calibration performed as part of thepotential probably requires additional complexity to exclude an unphysical source reconstruction. In practice we flagged reconstruction had an absolute value □ □ 10% of the peak positive pixels for additional scrutiny.

We perform extensive tests of the effective sensitivity and ward to infer an effective source-plane resolution or sensitivity from the observed (image plane) data. For example, the effective resolution and sensitivity vary with location in the source plane based on the local lensing magnification, and the source regularization strength depends on both the resolution and sensitivity of the original data. This becomes even more complicated when considering absorption components because orthogonal components of the lens ellipticity. Where necessary, the detection of absorption requires the presence of continuum emission,but the continuum brightnesabsorption depthand effective resolution and sensitivity allvary across the source plane. Following \$18, we perform a series of reconstructions of mock data to testthe resolution and sensitivity of the source reconstructions.

Briefly, we create many mock observations of pointlike background sources tiled across the source planænalyzing these fake data in an identical way to the real data. The intrinsic flux density of the artificial sources is setsuch that the total apparent(magnified) flux density matches that of the real Suyu et al. 2006; Hezaveh et al. 2016). The best-fit strength of sources (since these sources were selected in part based on their apparent brightness). We then fit the source reconstructions of each set of fake data with a two-dimensional Gaussian, taking the FWHM as an empirical estimate of the resolution of the the lensing caustics with magnifications □50We associate

these failed solutions with too-pooresolution in the sourceand image-plane pixegrids, because the pixesizes of these grids were not optimized for such extreme cases of high magnification and compact source sizes. Finally, we repeat this impact on our reconstruction apart from leaving residuals entire procedure but change the input flux density of the sourcen the model-subtracted data from the imperfectly subtracted to be a factor of 2–3 weaker than the faintest component in thelens emission. real absorption reconstructions in ordeto test the ability to recover input fluxes fainter than those actually observed is final test shows that even these weak signals are recoverable to ≈25% accuracy.

In summary, these tests lead us to conclude that the structures seen in the source reconstructions are ænd that absorption signals few times weaker than those actually observed can be successfully recover by the find no evidence that the lensing reconstruction procedure introduces artificial clumpy structure. The sources in our sample are resolved over~0."15. These data proved too shallow given their high spatial ≈5–20 independent resolution elements, in agreement with the resolution, and we excluded them from all of our analysis. image-plane data (Figure 2).

For the purposes of Figure 6 we illustrate the effective source-plane resolution with an ellipse based on the fits to the artificial data atthe position corresponding to the peak of the actualreconstructed source continuum emissiball maps of the effective resolution are provided in the Appendix.

# 3.4. Notes on Individual Sources

Our sample shows very diverse characteristics in terms of both lensing geometry and OH 119 µm line profiles some cases requiring special treatment. Here we give a brief summary of these particularities and comment on the conclusions we draw from the OH spectra.

## 3.4.1.SPT0202-61

The OH spectrum of this source clearly requires two velocity components to reproduce the dataThe [C II] profile of this source is also very broad and shows two peaks, likely indicating a major merger. The deepestOH absorption is redshifted compared to one of the peaks and blueshifted relative to the other. It is thus possible thatwe are seeing a molecular outflow (launched from the fainter [Component) or a molecular inflow (falling toward the brighter [C] peak), or simply strong systemic absorption from the interaction/ overlap region. The [0] data will be analyzed in future work and a detailed comparison between the extended and the OH absorption (confined to the continuum emitting region by definition) is complicated, but initial modeling does not conclusively point to an outflow. We thus consider this source ambiguous and do not claim a molecular outflow.

Additionally SPT0202-61 nearly uniquely among the SPT DSFG sampleshows submillimeter emission as center of the Einstein ring of background source emissionhis is most clearly visible in Figure 2. The available data make clear that background source. There is an additional unlensed continuumens potentials we find. source located □ 25 southwest of the lensed source, also noted by Spilker et al. (2016b). These sources willbe explored in more detailin future work. The pixellated reconstruction tool we employ does not have the ability to model lensed and unlensed emission simultaneouslyo we model and subtract the lens and secondary source before lens modelling lens emission does not cleanly separate from the lensed backgrounaddition to the lensed galaxythis source shows ateast two emission, so the subtraction is imperfect. o mitigate this, we

carefully define the image-plane and source-plane pixel grids in the lensing code such that to source-plane pixels map to the center of the Einstein ring. We have verified that this choice has

### 3.4.2.SPT0418-47

This source shows a cleabut not especially deep outflow component extending well beyond the high-S/NIJEmission. We note that this source was observed in ALMA projects 2015.1.00942.S and 2018.1.00191TSe 2015.1.00942.S data were taken with the array in a much more extended configuration than we originally requested, yielding a synthesized beam

## 3.4.3.SPT0441-46

The OH absorption atsystemic velocities is deeper in this source than in any otherin our sample, but the spectrum is better fit with an additional blueshifted velocity component. While the [C II] spectrum of this source is also broad and double-peaked like SPT0202-61unlike that source the OH absorption continues beyond the bluest [@mission. We can thus unambiguously confirm that this source hosts a molecular outflow. The deepestOH absorption is slightly redshifted compared to the [CII] peak, possibly indicating a molecular inflow toward the [CII] peak.

The lens model of this source required low-order multipoles to adequately reproduce the data. The best near-infrared image of the lens galaxy, from Hubble Space Telescope/WFC3 imaging, shows a second source ~1" west f the main lens galaxy. We do not know whether this second source is associated with the main lens galaxy, but it may be the cause of the additional complexity in the lens model required to fit the data.

# 3.4.4.SPT0459-58

The OH spectrum of this source shows very deep blueshifted absorption, and does not require multiple velocity components to fit the spectrum (mostly because the absorption is so broad that any additional velocity components are indistinct).

The continuum image of this source shows a morphology that is clearly inconsistent with a single simple lensing potential, which went unrecognized in earlier analysis due to the much lower sensitivity and resolution of the earlier data (Spilker et al. 2016b). The northernmostlensed image in particular requires that a second lens potential be placed in its vicinity in order to reproduce the image splitting at that location. Unfortunately the quality of the best available near-IR image of this source, from Very Large Telescope/ISAAC, is the central emission is not a (demagnified) lensed image of the poor to confirm or refute optical counterparts to the best-fit

# 3.4.5.SPT0459-59

The OH spectrum of this source shows no obvious evidence of additional blueshifted absorption beyond the broad CO emission, and we do not classify it as an outflow source. In other weakly lensed sources, one just south of the lensed

emission and the other ~15 southwest of the lensed emission. We do not detect OH absorption from either of these sources but they are faint in the continuum so it is unclear whether they are physically associated with the lensed source. Observations of an emission line at high spatial resolution could clarify the structure of the galaxy and allow for a better characterization of the OH absorption. In our modeling of this source, we subtracted the southwestern source prior to lens modeling in order to allow for more computationally feasible image- and source-plane pixel grids. uous outflow (including SPT2319-55 published by \$180he This also enables better source-plane regularization, since the remaining three sources allaye broad and/or double-peaked fitting for the regularization strength need notbe influenced by both the strongly lensed main source and the very weakly lensed southwestern source.

#### 3.4.6.SPT0544-40

The OH spectrum of this source shows a straightforward, albeit broad, blueshifted absorption profileWhile this galaxy appears to be a standard quadruply imaged background source at first glance, both the flux ratios and the spatial extent of the images make clear that it must instead contain two continuum components It is possible that these two continuum components both contribute to cause the overall broad absorption lin profile.

## 3.4.7.SPT2048-55

absorption and a weak blueshifted absorption component, and the outflows that do not intersect the line of sight toward stacked CO lines used as a reference do not have particularly the galaxy continuum. S/N. The outflow in this source is the weakestof those we consider unambiguous.

# 3.4.8.SPT2103-60

Similarly to SPT0459-59the OH absorption in this source does not show an unambiguous outflowing componembile the absorption troughs are blueshifted compared to the fluxweighted mean redshift of the CO emission still possible to the bluest part of the CO emission.

This source is also known to be lensed by a small group of galaxies three of which are required in order to reproduce the data (Spilker et al. 2016b). We note that we do not require the fractions but a high detection rate. These two scenarios are in the near-IR in either absolute or relative astrometreince the baryonic and dark-matter massescan become spatially decoupled in overdense environments. In particular the best-fitDSFG sample with the low-redshift comparison samples mass and position of the southwestern lens are degenerate.

# 3.4.9.SPT2132-58

as narrow systemic absorption, only barely reaching back to the lowest AGN fraction, f<sub>AGN</sub>□<□0.athough this difference is continuum level at the blue end of the ALMA bandwidth. This source was also studied in detalby Béthermin et al. (2016), who found a high excitation in the CO(12-11) transition that could be due to the presence of an AGN.

# 3.4.10.SPT2311-54

This source showsvery broad and extremely blueshifted absorption. This galaxy hosts the fastest outflow of our samplerate in the early universeFollowing Veilleux et al. (2013) in although the maximum outflow velocity is obviously uncertain assuming thatall galaxies in our sample have a biconically

since the limited ALMA bandwidth does not extend far enough to capture the full absorption profile.

## 4. Results

## 4.1. Molecular Outflow Detection Rate

We detect 119 µm OH absorption in 100% of our sample. and in 8/11 cases associate this absorption with an unambig-CO or [CII] line profiles that make it difficult to interpret the OH absorption. Assuming binomial statistics, the outflow detection rate is 73%  $\Box \pm \Box$  13% source shows evidence of OH in emission at systemic velocities; our ability to detect redshifted emission as in the classic P Cygni profile is limited due to the small ALMA bandwidth.

The overall high outflow detection rate demonstrates that molecular winds in these highly star-forming objects are very Common. Additionally, becauseOH as an outflow tracer manifests in absorption and because the absorption is highly optically thick (e.g., González-Alfonso et al. 2017), our high detection rate also implies that the opening angle of outflowing ematerialmustalso be high (otherwise the outflows would not be detectable in absorption because mixes of sight would not intersect outflowing gas)Our detection rate is therefore a lower limit on the true occurrence rate of molecular winds in Much like SPT0441-46, this source shows very strong syster → □ 4 DSF Obsecause there are presumably some sources

Even without performing any lensing reconstructionsor other spatial analysis, we can infer some details about the spatial structure of these outflows. In one possible scenario, large galaxy-scaleoutflows are being driven with a high opening angle so thatnost sources have a wind detectable in absorption due to the high covering fraction of outflowing material. Alternatively, it may be that the outflows are launched such that they are viewable along most lines of sight even with a small covering fraction. For example, if spherical outflows that the absorption is simply at systemic velocities with respectare preferentially launched from the nuclear regions of the host galaxies, we would nearly always detect an outflow even if the molecules are halted or destroyed before reaching kiloparsecscale distances from the nucleus, resulting in low covering positions of these lens galaxies to align with galaxies detected distinguishable using our lensing reconstructions of the windabsorbing material.

Figure 4 compares the outflow detection rate of our  $z\Box > \Box 4$ (Section 2.4). Our detection rate is very similar to that of z□<□0.3 IR-luminous galaxiest much higher than that of lower-luminosity AGN. We find a slightly higher detection rate This source shows very broad blueshifted absorption as well, when considering only the low-redshift ULIRGs with the not statistically significant. Figure 4 also shows the outflow detection rate as a function of Lcombining all available lowredshift OH samples. We do not find a decrease in the detection rate among the most luminous galaxies, a marginally significant difference compared to the low-redshiftsamples. Although the high outflow detection rate in our very luminous high-redshift sample was not unexpected, our observations place the firststatistical constraints on the outflow occurrence

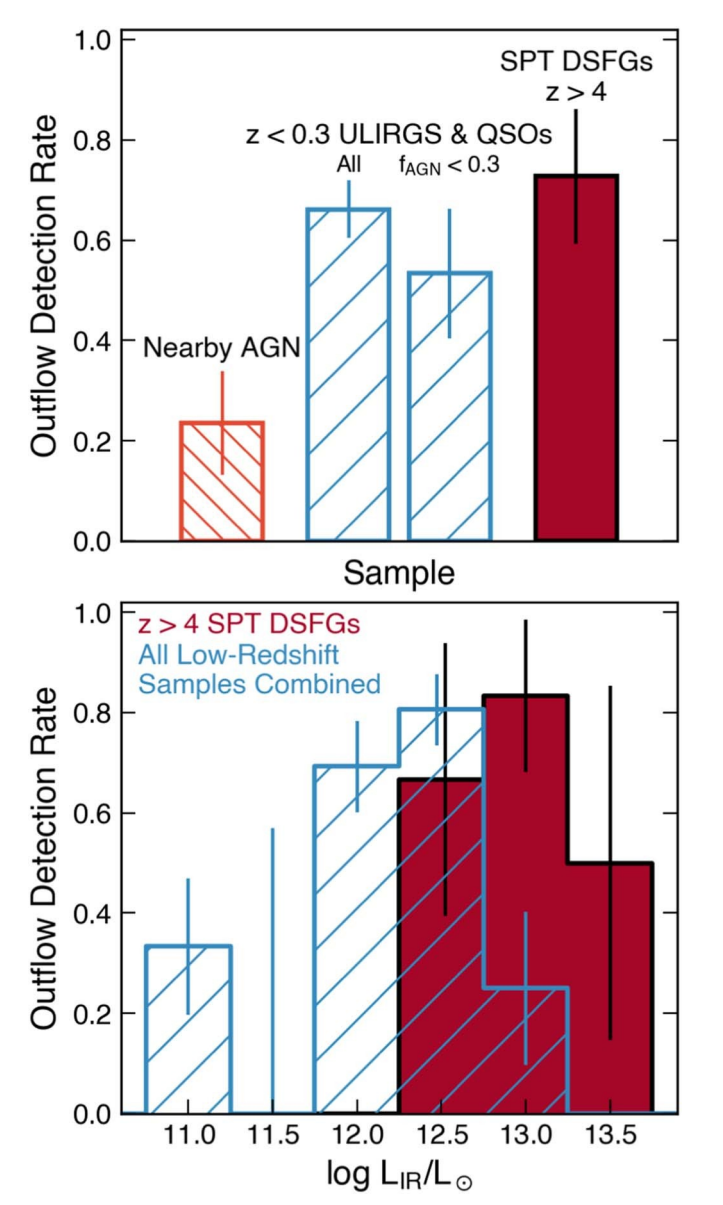


Figure 4. Top: comparison of outflow detection rates via blueshifted OH absorption between our high-redshift DSFGs and a compilation of low-redshift cannot reject the hypothesis that the two samples are drawn samples (Section 2.4). The high detection fraction we find is very similar to that from the same underlying distribution in any of the three in low-redshift ULIRGs. Uncertaintiesassume binomialstatistics. Bottom: outflow detection rates as a function of LAlthough the number of sources is small, we do not find a decrease in the detection rate in the mostuminous galaxies.

expanding outflowour detection rate would correspond to an opening angle of ~150°, again very similar to the 145° inferred to the edge of the observed bandwidth and could plausibly by Veilleux et al. (2013) or the 125° we infer for the lower subsample of all local objects.

Finally, we note that no source shows unambiguous evidence for molecular inflows, which would manifest as redshifted absorption profiles Two sources show  $y_0 \square \square + 50$ km s<sup>-1</sup>, sometimes used to classify sources as showing evidence for inflows; our criticisms of this metric when applied for one of the two doublet lines (i.e., should be multiplied by 2 to outflows also hold here (Section 3.2) In our sample, both sources have clearly double-peaked | Profiles, often a sign of mergers. It is unclear whether the slightly redshifted absorption we see is due to inflow toward one of the velocity components, outflow from the other, or simply systemic absorption from the putative interaction region between them.

The inflow detection rate in low-redshift ULIRGs is ~10% (Veilleux et al. 2013; Herrera-Camus et al. 2020) using the v metric, far lower than the outflow detection rate. Given the ambiguity in our data and small sample size cannot draw strong conclusions on this pointbut there is no immediately obvious difference between the inflow detection rates at  $z \square \sim \square 0$ and  $z\Box > \Box 4$ .

# 4.2. Basic OH Absorption Properties

We detect OH in absorption in all 10 target DSFGs (11 including the source in \$18); no source shows OH in emission or P Cygni profiles. While observational estrictions preclude us from detecting P Cygni profiles, the lack of OH in emission in any source is interesting because OH 119 µm appears in emission primarily in AGN-dominated galaxies  $\& f_N \square \square \square 0.8$ : e.g., Veilleux et al. 2013; Stone et al. 2016; Runco et al. 2020). For example, in the sample of Stone et al. (2016) of nearby AGN-dominated galaxies, >70% of the detected objects showed either pure emission or emission/absorption composite spectra, with 60% purely in emission. A similar conclusion applies to the more IR-luminous ULIRGs and QSOsbjects with  $f_{AGN}\square > \square 0.8$  typically show OH in emission (Veilleux et al. 2013). This is presumably because the dense nuclear regions are able to excite the 119 µm energy levels in spite of the very high gas densities required for collisional excitation, ~ 108 cm<sup>-3</sup> (Spinoglio et al. 2005; Runco et al. 2020). This may also be an evolutionary effect, where wide-angle outflows have cleared the sightline to the dense nuclear region and already subsided (e.g.Veilleux et al. 2013; Stone et al2016; Falstad et al. 2019). The fact that we do not see OH in emission in any of our sources is a secondary empirical indication that AGN are probably not dominant in these galaxies, unless the column densities are so high as to be optically thick in the mid-IR in the direction of the emitting regions.

Figure 5 shows histograms of three differentetrics of the OH absorption velocity  $v_{50}$ ,  $v_{84}$ , and  $v_{max}$ , for our sample and literature sources. We exclude those sources for which OH was detected only in emission. We find very similar distributions of these quantities between the low- and high-redshift samples. A two-sided Kolmogorov-Smirnov (K-S)test confirms that we velocity metrics. While it appears that the low-redshift sample has a tail to extremely fast maximum outflow velocities  $V_{\text{max}}$  - 1400 km s<sup>-1</sup> that is not present in our data, the limited ALMA bandwidth means we could not probe such high velocities if they were present in our sample. Indeed, two of our sources show absorption that continues essentially all the way reach higher outflow velocities than the extrapolations from our fits to the spectra suggestippending on the true line profiles.

Figure 5 also shows the equivalentwidth distributions of these samplesand the relationships between the equivalent widths and the velocity metrics. The equivalent widths are the total values (systemic plus any red- or blueshifted absorption) for the total equivalent widths). The equivalent width distribution does show a significant difference between the low- and high-redshiftsamples; a two-sided K-S test rejects the hypothesisthat the two samples are drawn from the same underlying distribution (p = 0.004). This appears to be because the SPT DSFGs show stronger OH absorption than

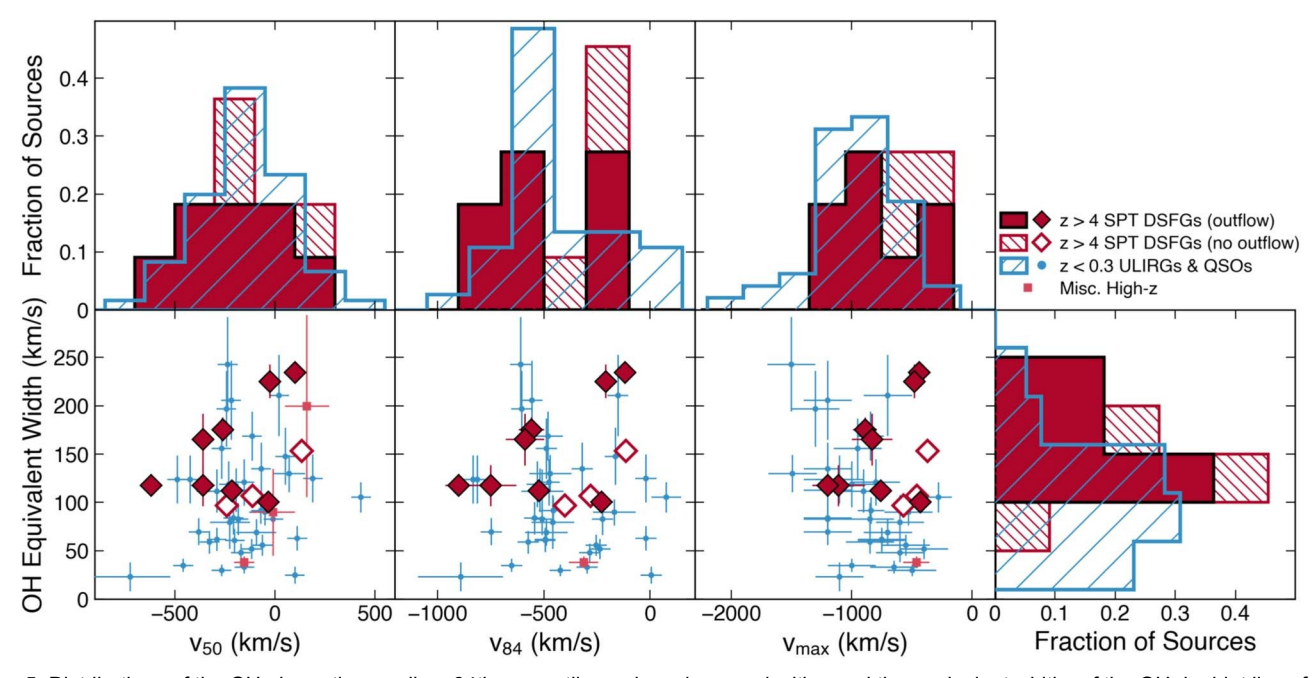


Figure 5. Distributions of the OH absorption median, 84th percentile, and maximum velocities and the equivalent widths of the OH doublet lines for our sample and literature sources. Histogram bins have been slightly offset between the samples for clarity. The limited ALMA bandwidth would prevent us from detecting the faste outflows seen in the low-redshift samples. Not all literature studies report all quantities in this figure, so there are some discrepancies between the histograms and scatter plots. In particular Spoon et al. (2013) (a subset of the "z <a href="Color: ULIRGs">Color: ULIRGs</a> and QSOs") do not provide equivalent widths; this sample is noticeably absent from the "z <a href="Color: ULIRGs">Color: ULIRGs</a> and QSOs") do not provide equivalent widths; this sample is noticeably absent from the "z <a href="Color: ULIRGs">Color: ULIRGs</a> and QSOs") do not provide equivalent widths; this sample is noticeably absent from the "z <a href="Color: ULIRGs">Color: ULIRGs</a> and QSOs") do not provide equivalent widths; this sample is noticeably absent from the "z <a href="Color: ULIRGs">Color: ULIRGs</a> and QSOs") do not provide equivalent widths; this sample is noticeably absent from the "z <a href="Color: ULIRGs">Color: ULIRGs</a> and QSOs") do not provide equivalent widths; this sample is noticeably absent from the "z <a href="Color: ULIRGs">Color: ULIRGs</a> and QSOs") do not provide equivalent widths; this sample is noticeably absent from the "z <a href="Color: ULIRGs">Color: ULIRGs</a> and ULIRGs and ULIRGs and ULIRGs are the "z <a href="Color: ULIRGs">Color: ULIRGs</a> and ULIRGs are the "z <a href="Color: ULIRGs">Color: ULIRGs</a> and ULIRGs are the "z <a href="Color: ULIRGs">Color: ULIRGs</a> and ULIRGs are the "z <a href="Color: ULIRGs">Color: ULIRGs</a> and ULIRGs are the "z <a href="Color: ULIRGs">Color: ULIRGs</a> are the "z <a href="Color: ULIRGs">Color: ULIRGs</a> and ULIRGs are the "z <a href="Color: ULIRGs">Color: ULIRGs</a> are the "z <a href="Co the plot of equivalent width  $vsV_{max}$  compared to the  $the_{max}$  histogram.

the low-redshiftsamplesbeing underrepresented at equivalent widths and overrepresented at high equivalent widths.

selection effects. While it is plausible that weak absorption would be more easily detected in the brightnearby samples than in our very distanttargets,OH was strongly detected in every SPT sourceWe could have detected equivalentidths ~5× lower than even the weakest absorption actually seen; theabsorption reconstructions are most reliable. dearth of weak OH absorption in the high-redshifsample is genuine. The differences in typicaLIR and fAGN between the same two-sided K-S testreturns p□=□0.02 when considering consists of multiple sources poorly resolved by the present only the low-redshift sources with higher LR than our leastluminous sourcelog( $L_{IR}/L_{\Box}$ ) 1 12.5, and p $\Box$ = $\Box$ 0.04 for only the low-redshift sources with  $f_{SN} \square < \square 0.4$  (the number of lowredshift objects that are both very luminous and have low f is too small for a meaningful comparison). We conclude that OH absorption at high redshift does appear to be genuinely stronger than in similar low-redshift galaxies, but a more complete sampling of objects at lower-Land/or higher fagn at high redshift is required to make a more thorough comparison.

# 4.3. Continuum and Absorption Reconstructions

and the OH absorption component(s) for each source, presenting the absorption mapsin terms of both integrated absorbed flux and equivalent width. While absorption is a multiplicative and not an additive process, our ability to detect absorption is not. Consider for example a region with continuum S/N□~□@re would likely not confidently detect absorption even in the case of 100% absorption, while far weaker absorption is detectable where the continuum is brightest. We mask the maps of absorbed flux in regions

where the continuum is detected at  $S/N\square < \square 5$ . Even above this threshold in most sources we find some pixels in the absorption This difference cannot be explained by simple observational maps with positive flux (or negative equivalent width), which is simply a reflection of differencing two moderately uncertain measurements. These positive regions are mostly eliminated if we change the threshold to continuum S/N□>□\mathbb{\text{\text{\$\text{\$0\$}}}} \int \text{\text{\$\text{\$\text{\$\text{\$\text{\$\text{\$\text{\$}}\$}}}} \text{\text{\$\exitt{\$\text{\$\text{\$\text{\$\text{\$\text{\$\text{\$\text{\$\text{\$\text{\$\exitt{\$\text{\$\exitit{\$\text{\$\text{\$\tex{\$\text{\$\}}\$}}\text{\$\text{\$\text{\$\text{\$\text{\$\text{\$\text{\$\ consider to be an empirical ndication of the level where the

The continuum emission in our sources is mostly smooth at the resolution of these observations, with effective circularized two samples also do not explain the different distributions. The radii r<sub>cont</sub>□≈□0.5–4 kpc (the largest source, SPT0459-59, clearly data). These sizes are similar to or somewhat smaller than those found by Hodge et al. (2016) in a sample of unlensed DSFGs at lower redshiftbut typical for the lensed SPT DSFGs (Spilker et al. 2016b), although the methodology forestimating size differs between these works A few sources show multiple peaks in the continuum reminiscent of mergers, but we see little evidence for distinct sub-kiloparsec substructure. Recent ALMA observations of lensed and unlensed galaxieshave demonstrated that dentifying clumps in dustemission can be precarious even in data with  $S/N \square \square \square 30$  because the relevant metric is the contrast between the clumps and the underlying smooth emission (e.g.Hodge et al. 2016, 2019; Rujopakarn Figure 6 shows the lensing reconstructions of the continuumet al. 2019; Ivison et al. 2020). Our observations typically reach peak S/N values far higher than these studies, but the substantialfreedom afforded by the pixellated lensing reconstructions reduces the effective peak S/N in the reconstructions to □~25-40 for all sources. That is, there is no direct correspondence between image- and source-plane S/N because our lensing reconstructions fully accounter the uncertainties in the data rather than directly map from image to source. We rule out significant 500 pc scale clumpinessin our sample at □ □ 10% of the total flux density as seen in some ALMA

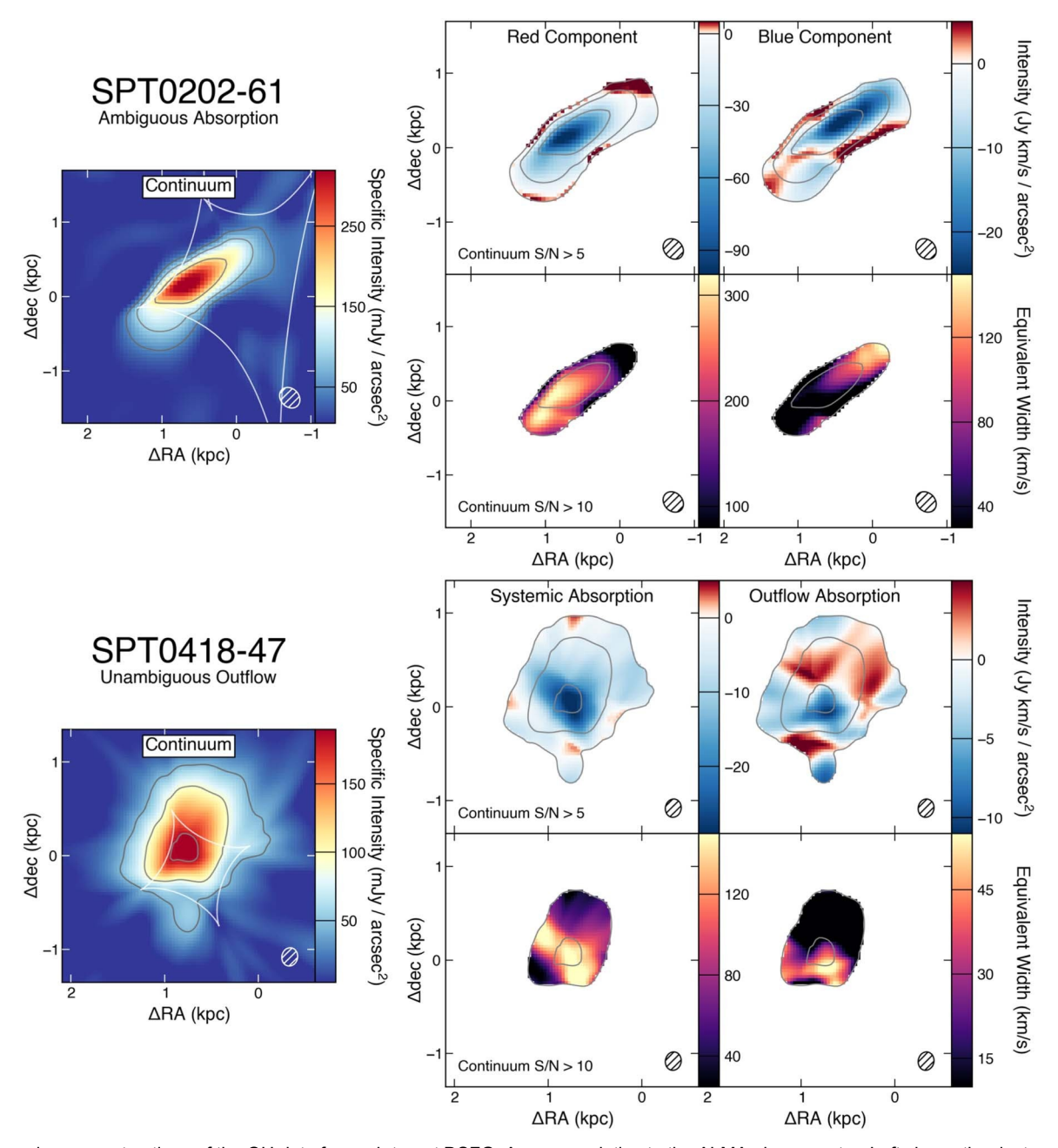


Figure 6. Lensing reconstructions of the OH data for each target DSFG. Axes are relative to the ALMA phase center. Left shows the dust continuum emission with gray contours overlaid aS/N of 5, 10, and 20; these contours are repeated in the other panels lensing caustics are shown in white ight panels show the reconstructions of the OH absorption component(s) as indicated in Figure 3 and listed in Table 3. Upper rows show maps of the integrated absorbed flux density w lower rows show maps of the equivalent width. We mask the upper rows for continuum S/N□ <□ 5 and the lower rows for continuum S/N□<□ 10. At lower right each panel we show an ellipse representing the effective spatial resolution of the reconstructions at the peak of the reconstructed continuum densities patrial resolution varies across the source plane; see Section 3.3.1 and the Appendix.

studies (Hodge et al. 2019) but cannot rule out weaker and/or smaller clumps.

peaks near the same location as the continuum, with an equivalent width distribution that can be either centrally concentrated or more widespread and uniforn he systemic absorption tends not to show signs of distinct clumps, like the continuum emission. This is altogether unsurprising, given that systemic absorption distinct clumps or small-scale substruc-OH is sensitive to even fairly small column densities of moleculargas, which is satisfied overlarge regions of these gas-rich galaxies busubjectto line-of-sight geometric effects (e.g., González-Alfonso et al2017).

The outflow maps show more interesting structure when visualized in terms of either absorbed flux or equivalent width. In sources with systemic absorption, the absorption generallyn contrast to the systemic absorption, the blueshifted outflowing gas rarely peaks in equivalent width at the locations of the continuum peaks, instead often showing the largest equivalent widths significantly offset from the brightest continuum emission Also in contrast to the continuum and tures are common in the molecular outflows. Combined, these two facts may indicate that the high-velocity gas has already moved away from the nuclear regions and now appears offset (if indeed the outflows were launched from the nuclear

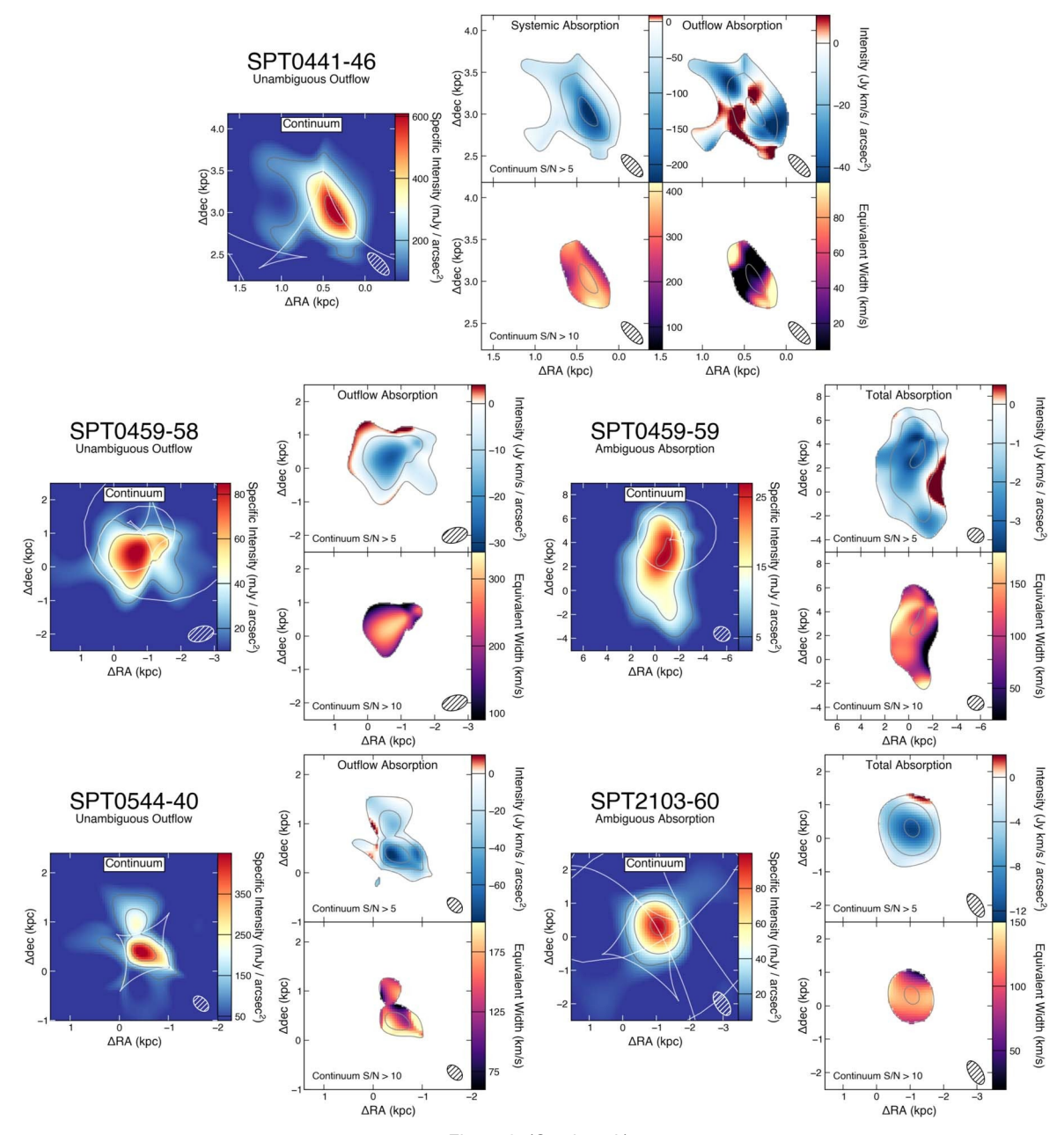


Figure 6. (Continued.)

regions), similar to the offsets commonly seen between the core19 µm absorption is expected to be very optically thic We and high-velocity CO emission in low-redshiftutflows (e.g., Lutz et al. 2020). Alternatively, it could be that high-velocity outflows are more easily launched in regions with lower column densities than the very dense nuclear regions (e.g., Thompson & Krumholz 2016; Hayward & Hopkins 2017).

Figure 7 shows the absorption covering fraction for the reconstructions in each source, defined as the fraction of pixels orrelation rules out that the absorbing material as a typical in the reconstructionsof equivalent width with detectable high covering fractions ranging from 30% to 85% for the outflows or 40% to 95% for the systemic absorptionThese values are typically somewhallower than the overall sample detection rate of 73% for either component out significantly spectra. This may be somewhat surprising given that OH

return to this comparison in Section 5.1.

Figure 8 searches for trends of absorption covering fraction with selected other quantities we have measured. First, we find no correlation between the covering fraction of either systemic or outflow components with the actual physical size of the dust continuum emitting region (Figure 8 left). This lack of constantphysical size. If this were so, we would expect the absorption where the continuum  $S/N\square > \square 10$ . We find generall vovering fraction and continuum emitting size to be inversely correlated, with the typically sized absorbing regions covering a larger fraction of intrinsically smaller galaxies.

Second, we do find intriguing evidence for a correlation between the outflow covering fraction and L with the most higher than the fractional absorption depths in the apparent OHuminous sources showing higher covering fractions (Figure 8 right). Taken at face value, this result implies that more

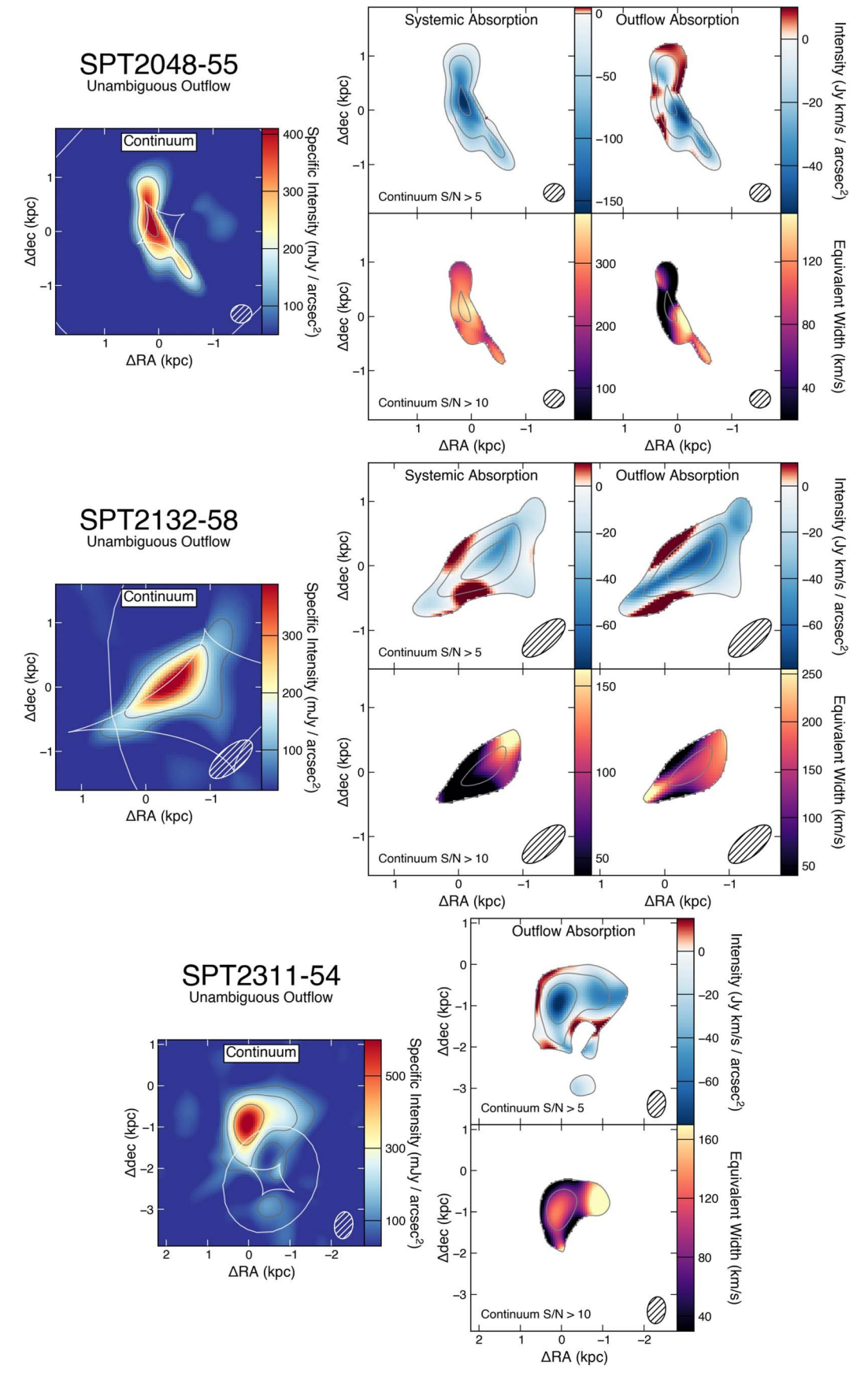


Figure 6. (Continued.)

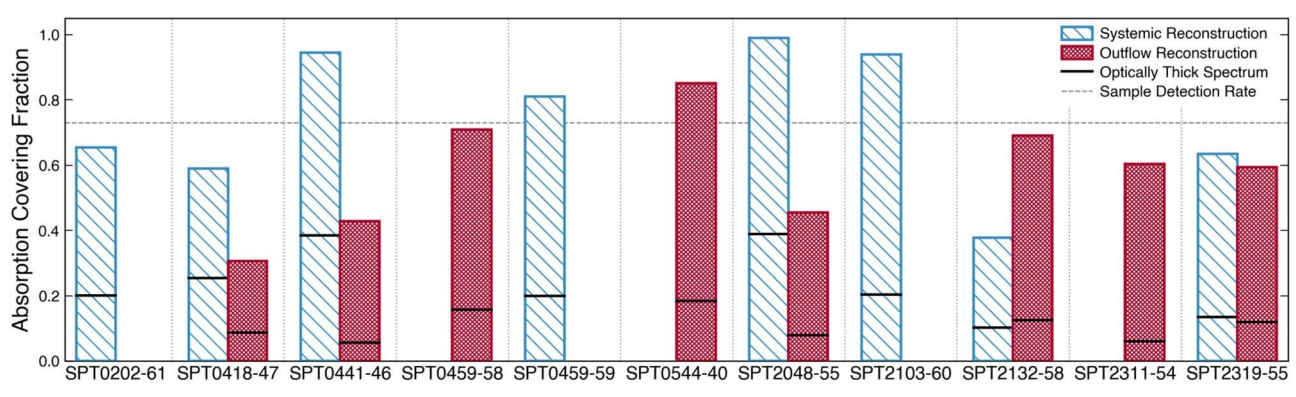


Figure 7. Covering fractions of OH absorption from the reconstructions of each source fined as the fraction of pixels with detectable absorption where the continuum S/N = 16 orizontal black lines show the expected covering fraction derived from the absorption depth over the velocity range arch modeled component assuming optically thick absorption these representand lower bounds on the covering fraction. In the dashed gray line shows the sample-averaged detection rate of 73% (which is the same for the outflows and systemic absorption). The differences between these values may imply the presence of substructure absorption on scales several times smaller than the resolution our data provides; see Section 5.1.

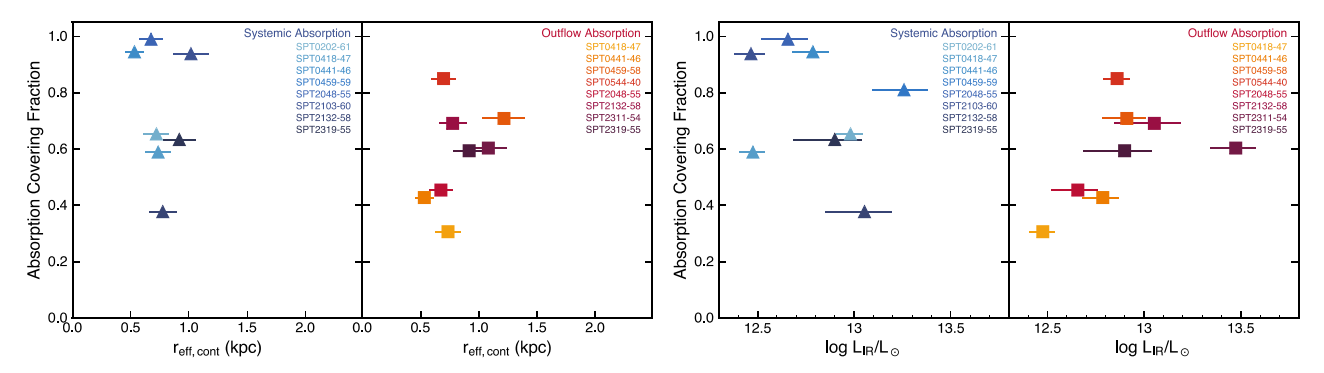


Figure 8. The mostIR-luminous sources in our sample have higher outflow covering fractionsplying that these galaxies are able to launch more widespread outflows. The figure shows the OH absorption covering fractions from the lensing reconstructions against the effective dust continuum emitting sizes (Left) and L (right). The lack of an inverse correlation with the continuum size rules out that the absorbing structures have a typical constant physical size, but there is an intrigu correlation between covering fraction and L

luminous galaxies are able to launch more widespread outflows, with either larger opening angle or more and/or larger clumps. At some level this result is also consistent with the trend of outflow detection rate rising with L IR, which extends over a larger dynamic range in than probed by our sample alone (Figure 4)n order to see such a trendone can invoke either a rising outflow occurrence rate or an increasing outflow covering fraction with LIR, or both. The same trend does not exist for the systemic absorption components, implying (unsurprisingly) thatthe covering fraction of gas at rest is dependent on the line-of-sight geometry but not necessarily any intrinsic physical properties of the galaxies.

For the sources that show unambiguous outflows onlyin Figure 9 we additionally find correlations between the outflow covering fraction and the outflow velocities  $y_0$  and  $v_{max}$ . In addition to being driven by the most luminous sourcesthe galaxies with high covering fractions also show the fastest outflows. Some of this is no doubt driven by underlying trends we find between  $L_{IR}$  and  $v_{50}$  or  $v_{max}$  for the sources in our sample with outflows, as we explore in more detail in Paper II. "clumpiness" in the reconstructions, we borrow several metrics It is intriguing nonetheless that the outflow covering fraction appears to be correlated with either or both quantities. Whetherlumps and mergers in high-redshiftalaxies (e.g. Lotz et al. these trends hold with increased sample sizes that span a wide 2004; Law et al. 2007; Förster Schreiber et al. 2011; Wuyts dynamic range in hostproperties is an interesting motivation for future investigation.

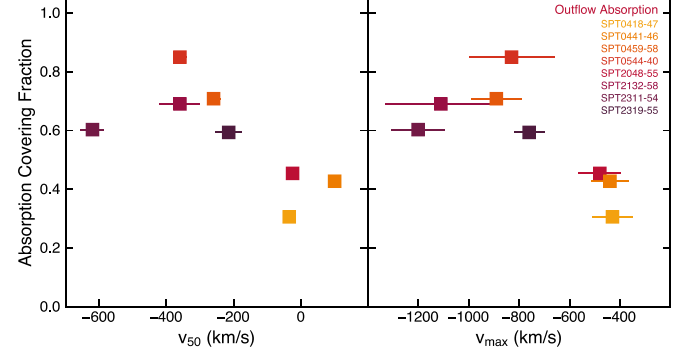


Figure 9. The galaxies with the fastest outflows also show the highest covering fractions or most widespread outflows. We show the lens model covering fractions against<sub>50</sub> and  $V_{\text{max}}$ , plotting only those sources with unambiguous outflows

## 4.4. Ubiquitous Clumpy Molecular Outflows

In an effort to further quantify the degree of small-scale from the extensive literature on morphological analyses of et al. 2012; Guo et al. 2018). Specifically, for the continuum and absorption component(s) of each source, we calculate:

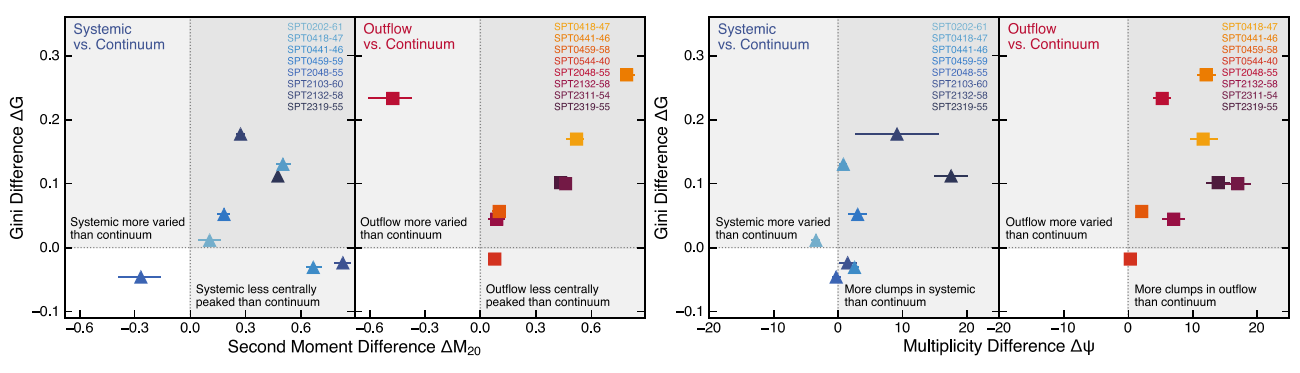


Figure 10. The molecular outflows in our sample are clumpier than the continuum emission, and generally clumpier than the systemic absorption as well. We show  $\label{eq:difference} \textit{(absorption minus continuum) of the Gini coefficient G, second-moment para} \textit{para} \textit{(absorption minus continuum) of the Gini coefficient G, second-moment para} \textit{(absorption minus continuum) of the Gini coefficient G, second-moment para} \textit{(absorption minus continuum) of the Gini coefficient G, second-moment para} \textit{(absorption minus continuum)} \textit{(abs$ differences are stated on the plots; sources in the upper right quadrant can be considered to have clumpier structure in the absorption than the continuum by multi metrics. The molecular outflows are significantly clumpierin general than the continuum, with 6/8 sources considered so by all three metrics. The systemic absorption on the other handis generally less clump with only 3/8 sources showing significant differences in all three metrics.

(1) the Gini coefficient G (Abraham et al. 2003), which quantifies how uniformly the pixel values in an image are distributed, ranging from 0 if all pixels are equal, to 1 if a single eight outflows by all three metrics. The systemic absorption pixel contains all the flux; (2) the second-order moment of the components on the other handare less clearly clumpier than 20% brightestpixels M<sub>20</sub> (Lotz et al. 2004), which measures how centrally peaked the pixels in a source are, with high values indicating the presence of off-nuclear clumpand (3) the "multiplicity"  $\Psi$  (Law et al. 2007), sensitive to the presence outflows showing large differences  $\Delta\Psi\Box > \Box$  **5**etween the of multiple clumps of flux with higher dynamic range than, M where higher values indicate that an image contains more and reconstructions. or brighter clumps. As a reference for the dynamic range of these quantitiesG is by definition confined to the range 0-1. galaxies from the Sloan Digital Sky Survey, and Ψ ranges fromthemselves make cleathat the outflows are not uniform, as 0 to ≈30 in rest-frame UV images of z ~ 2 galaxies (Lotz et al. expected in a simple spherically expanding geometry. The 2004; Law et al. 2007).

We prefer these metrics as opposed to othernethods for severalreasons. First, they do not rely on subjective visual identification of clumps, and are deterministic and reproducimodels of the original data). Third, it is straightforward to compare these quantities between the absorption reconstructions and the continuum emission.

We calculate each of these quantities for the absorption and continuum reconstructions measured from the maps of equivalentwidth and for pixels where the continuum S/N => 10 (our conclusions are unchanged if we use the maps of absorbed flux instead). We calculate uncertainties for these measurementsthrough a Monte Carlo procedure, adding normally distributed noise to the reconstructions and remeasur-molecular outflows in the early universe, reaching typical ing G, M<sub>20</sub>, and Ψ, and taking the 16th–84th percentile range of the distributions as the uncertainty on the measured values tion allows some predictions to be made for the smaller-scale We measure the difference between the absorption and the continuum for each of these quantities to mitigate effects from the varying spatial resolution across the source planee; ause the same pixels are considered for both absorption and continuum.

Figure 10 shows the results of this procedure for the systemic and outflow absorption components of each source. This figure confirms what was apparentby eye from the reconstructions: the molecular outflows are significantly

clumpier than the continuum emission. All outflows would be considered as clumpier by aleast two metrics, and six of the continuum:only 3/8 sources show significant differences in all three metrics. The multiplicity Ψ shows the largest differences between outflow and systemic absorption, with 6/8 outflow and continuum, compared to only 2/8 of the systemic

From this analysis, we conclude that the molecular outflows in z□>□4 DSFGs are much more irregular on 500 pc scales than M<sub>20</sub> typically ranges from −3 to −1 in optical images of nearby the continuum emission. These metrics and the reconstructions maps of equivalent width show that the absorption is rarely strongest where the continuum is brightest, even though absorption is easiestto detect in those regions. Instead the equivalentwidth often reaches its maximum values in small ble. Second, they are non-parametric and do not rely on furtheclumps near the outskirts of the continuum emission, as might modeling of the reconstructions (which are themselves alreadybe expected in the case of either a clumpy expanding shell or a scenario in which the lowest column densities in the interstellar medium are more easily removed (e.g., Thompson & Krumholz 2016; Hayward & Hopkins 2017).

# 5. Discussion

# 5.1. Expectations and Prospects for Detecting Small-scale Clumpiness

We have presented the first sample of spatially resolved spatial resolutions □ ≈200–800 pthe physics of OH absorpstructure of the outflows, beyond our current resolution limits.

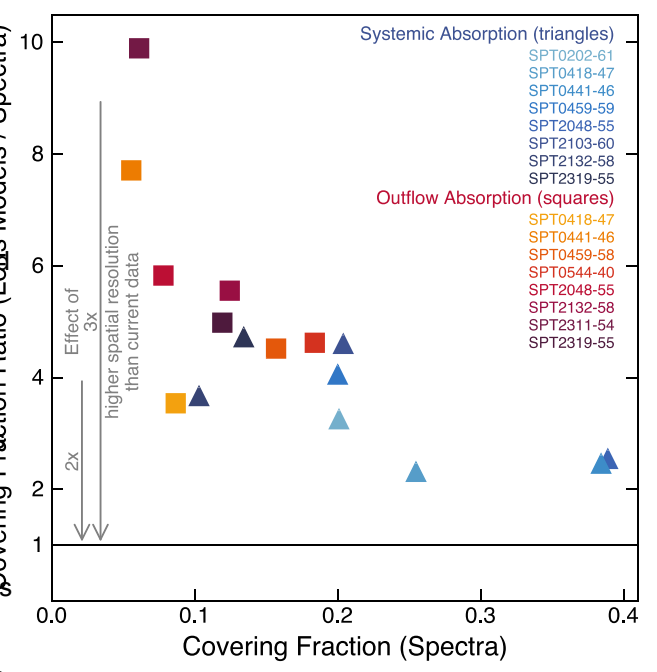
OH 119 µm absorption is highly optically thick in local galaxies, T<sub>OH119</sub>□□□10 even in the line wing **s**.g., Fischer et al. 2010); in effect, wherever OH is present along the line of sight ~100% of the 119 µm continuum light is absorbed. Alternatively, if we observe that, say, 10% of the continuum light has been absorbed from the OH spectra, we can infer that ≈10% of the continuum source is covered by absorbing OH molecules. For our sample, the outflow absorption components show depths of 5%–20%, which implies that only 5%–20% of the continuum emitting regions are covered by outflowing gas. These values are much smaller than either the overall detection rate (73%  $\pm$  13%) or the covering fractions from the lensing  $\sigma$ reconstructions. Figure 7 compares these three quantities. How can these values be reconciled?

Models The difference with the outflow detection rate is easiets: considerif molecularoutflows typically have some fortuitous geometry, then the detection rate and the covering fractions need not be similar. Considera simple scenario in which small sphericabutflows are launched from the nucleaegions of a ₽. population of galaxies. In this case an outflow would be detected in virtually every source and from every viewing angle even if the molecular outflows cover only a small fraction of the galaxies before being decelerated or destroyed. While our reconstruction do not necessarily supporthis geometry the arguments the same. There need nobe a correspondence between the typical outflow covering fraction and a sample-averaged detection rate

The comparison between the covering fractions inferred from ≥ the OH spectra and what we find from the lensing reconstructions has more interesting potential implications because now two differentestimates of overing fraction are being compared for individual galaxies. The differences between the two estimates in the molecular outflows would our sample span factors of 2–10, with the lensing reconstructions directly resolved at □3× better resolution than the current at a provide, always showing larger covering fractions. The reconstructions absesponding to 50-200 pc scales. The ratio of our measured covering show thatthe outflowing gas tends to be distributed in several distinct clumps at the spatial resolutions we achieve, but the individual clumps themselves are generally not spatially resolved tically thick. We implicitly assume that the spectra-based covering fractions While we cannotconclusively reconcile these two methods for are the "true" values and neglect any emission from dust in the outflows, which covering fraction with the data at hand, we briefly consider a fewould move the points downward on this plot. possibilities.

First, it is important to remember that the lensing reconstructions by galaxy NGC 4631However, even under the assumpuse data that span a wide range of velocities, using 300–700 km<sup>-1</sup> of bandwidth from the ALMA spectra. The clouds at many different velocities that cover only small fractions concile the estimates covering fraction in our sample. of the sources at any individual velocity but a much larger fractibhus, while we expect that some portion of the absorption of the source when considered as an ensemble scenario spatialresolution as we currently havallowing more detailed lensing reconstructions that bdivide the blueshifted line wings into narrower velocity bins.

from within the outflows, which would be particularly relevant if a large fraction of the total dust mass is contained in the outflows and/or if the dust in the outflows is substantially warmer than that in the galaxies. Cold dust has been detected expectthat if these outflows were observed attigher spatial a handful of local outflows (e.g.Leroy et al. 2015; Meléndez et al. 2015; Barcos-Muñoz et al. 2018), comprising □10% of separate the contributionsThis is insufficient to explain the gap between the outflow covering fractions from our OH spectra and reconstructions unless the dirsthe outflows is much warmer than that in the galaxies. Meléndez et al. (2015) outflows, the ratio between the two estimates of covering find that either higher dust temperatures a steeper dust emissivity index could explain the differences they observe between the dusemission in the disk and the outflow in the



fractions from the lensing reconstructions those from the OH spectra provides an estimate of the spatial resolution that would be required to directly resolve the absorbing substructure because OH is expected to be highly

tion that the emissivity plays no role, the dust in the outflow is only ~10% warmer than the dust in the disk, well short of reconstructions could thus represent the superposition of absorbing ~50%-100% higher temperatures that would be required to profiles has been filled in by emission from dust would be eminently testable with more sensitive data at the sargetflows, it is not likely to be enough to reconcile the difference in covering fractions we find.

Finally, it is very likely that the outflows we have observed contain substructure on spatiacales smaller than our current Second, the continuum could be "filled in" by dust emission resolution limits. Most of the clumpy structures in the lensing reconstructions are not individually spatially resolved; we only identify distinct clumps because they are separated from each other by more than our effective resolutionThus, we would resolution then the covering fractions in the lensing reconstructions would decrease, most likely in conjunction with any the total dust mass in the galaxies when it has been possible todecrease resulting from modeling narrower velocity bins in the outflows as well. Note that this implicitly assumes that the spectra-based covering fractions are the "true" values.

> Ignoring any re-emission of continuum from dust in the fraction corresponds the expected size scale required to resolve the substructures in the outflows. If we take the spectrum-based covering fractions as the "true" values, then the differences with our lens modeling results must be due to insufficient spatial resolution; higher-resolution observations would then yield lower covering fractions untilin agreement with the spectrum-based values. This is shown more clearly in Figure 11. This figure shows the ratio of the covering fractions

<sup>&</sup>lt;sup>19</sup> There is some wiggle room at the factor-of-two level allowed in this comparison if one allows significant turbulent velocity dispersion in the absorbing material at a given covering fraction, which effectively redistributes some amount of absorption to adjacent velocities; see González-Alfonso et al (2017), their Figure 3.

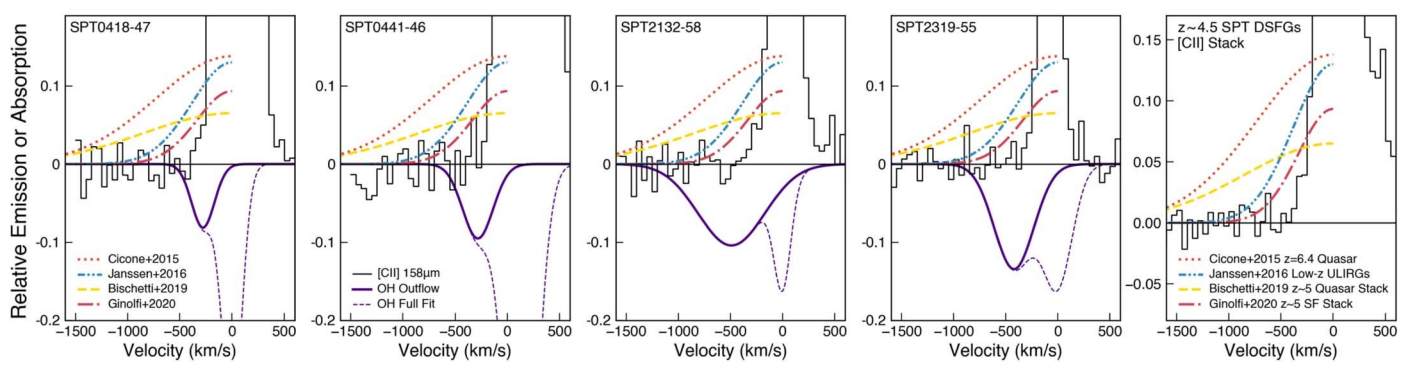


Figure 12. [C II] is at best an unreliable indicator of whether molecular outflows are present compare [OI] and OH for the four sources in our sample with unambiguous OH outflows and high-quality ALMA [0] data (left four panels) and the stacked [0] spectra of these four sources (rightmost nel). The [CII] spectra have been normalized to peak at 1. The OH best-fit absorption profiles have been normalized by the 119 µm continuum level and show only one of the doi components for clarity. Colored lines show several claimed outflows seen as broading wings in a z□=□6.4 quasar (Cicone et al. 2015), the median result for a sample of 22 nearby ULIRGs (Janssen at 2016), a stack of 22 z - 5.5 quasars (Bischettl. 2019), and a stack of 25 z - 5 star-forming galaxies (Ginolfi et al. 2020). We find no evidence for excess [emission at the velocities with clear blueshifted OH absorption. The S/N in our data rules putrios similar to these studies in individual sources and strongly excludes them in the stacked spectrum.

derived from the lens models to those from the spectra (or the high-redshift source or confirmed through deeper observations ratio of the bars to black lines in Figure 7). Assuming the OH absorption is optically thick, this ratio is a proxy for the spatial  $z\Box > \Box 4$  are fairly routine yeral groups have stacked the I[C] resolution that would be required to directly resolve the absorbing structures. We estimate that linear spatial resolution in evings indicative of outflows, with mixed success. 2-3 times better than the current data would be capable of resolving the absorption. Given the resolution and covering fractions measured in the currentata, we would predict that observed is of the order of 50-200 pWe note that similar estimate can be obtained simply by combining the covering fractions from the OH spectra with the observed continuum sizes. Even such small spatial scales are accessible with ALMhave found no or only marginal evidence for [CII] outflows in lensed objects given sufficient observational investment.

# 5.2. [C II] Is Not a Reliable Molecular Outflow Tracer

We have detected molecular outflows in a large fraction of the outflows are detected in absorptiogalaxies brightin the far-IR continuum are required, limiting us to dusty objects. The 2017; Herrera-Camus et 2020). rest frequency of the 119 µm doublet feature is also rather inconvenient because the atmospheric transmission limits observations to particularedshift ranges for z□<□6 galaxies and is inaccessible from the ground for  $z \square \square \square 2$ .

One potential alternative outflow tracer is [C II] 158 um. where the outflow manifests as excess emission in broad line wings at high relative velocities or as emission that does not follow the overall galactic rotation curve if high-resolution data are available.[C || ] is excited in a wide variety of gas conditions and arises from warm ionized eutralatomic, and molecular gas (e.g., Langer et al. 2014). In the nearby universe Ginolfi et al. (2020); the median SFR of those objects is more Janssen et al. (2016) find tentative correlations between the Othan an order of magnitude lower than that of our sample. outflow velocity and the broad [QI] line width and between the mass outflow rates derived from each tracer in a sample of [CII] spectra of our four targets, which again shows no ULIRGs and QSOs, suggesting that [Could prove a useful tracer of outflows at high redshift as well.

In the distant universe, a [C] outflow has been reported in an individual  $z \square = \square 6.4$  quasaraiolino et al. 2012: Cicone et al. 2015), although such bright [Q] line wings as in those works have not been replicated in any other individual

Four galaxies in our sample with unambiguous OH outflows also have high-quality ALMA observations of IQ (i.e., S/N that rivals or exceeds that of the stacking results above). These data will be analyzed in detail in future work. Figure 12 compares the OH absorption and [0] emission profiles of these four objects. No individual source shows evidence of excess [OI] emission at the velocities where we detectOH outflows. Moreover, [C II] wings similar to those reported in the literature would have been easily detected in all individual targets<sup>21</sup> with the possible exception of the stacking result

A still more stringentconstraintcomes from stacking the evidence for high-velocity [QI] emission, strongly excluding line wings similar to those reported in the literature (Figure 12, right). We construct this stack by subtracting a linear continuum from the integrated spectrum of each source

of the original target. Now that ALMA observations of [Cat spectra of various galaxy samples in an effort detectbroad Gallerani et al. (2018), Bischetti et al. (2019), and Ginolfi et al. (2020) each reportC ||] outflows in stacked spectra of, respectively,nine z□~□5.5 UV-selected star-forming galaxies the true size scale of clumps in the molecular outflows we have from Capak et al. (2015), 48  $4.5 \le \le 7.1$  quasars assemble from the ALMA archive, and 50  $z\Box \sim \Box 5$  star-forming galaxies from the ALPINE survey (Le Fèvre et al. 2020; Béthermin et al. 2020; Faisst et al. 2020). Other guasar studiesvever, despite many sources overlapping with the sample of Bischetti et al. (e.g., Decarli et al. 2018; Stanley et al. 2019), suggesting that perhaps residually stematic uncertainties in the stacking make the detection and interpretation of broad | Wings less straightforward.[CII] wings are also not seen toward an our sample, but OH is an inconvenient outflow tracer. Because individual z□~□6 quasar with a tentative OH outflow, although the [CII] sensitivity is too low to be conclusive (Shao et al.

in the beam area by a factor of 4-9.

<sup>&</sup>lt;sup>21</sup> To make the fairestcomparison in each case compare to the median properties of the sources of Janssen et al. (2016), the 2" aperture fit of Cicone That is, doubling or tripling the spatial resolution would result in a decrease et al. (2015), an average of the FWHM > 400 km bsets of Bischetti et al. (2019), and the SFR<sub>nediar</sub> $\Box = \Box 50_e \text{Myr}^{-1}$  result of Ginolfi et al. (2020).

excluding velocities |v|□<□500 km, segridding each spectrum to a common velocity frame, and normalizing each spectrum by the peak of the [0] emission before averaging. We tried a variety of other stacking procedures and continuum of C<sup>+</sup> but would reconcile the OH and [C II] observations. subtraction methods and found that our result is not sensitive to More importantly, it is almost certainly not true that OH is these details because the individual input spectra all have veryoptically thin (even the [C II] may have non-negligible line

At the very least, then, we must conclude that even if IC can be used as a molecular outflow tracetridoes nottrace it reliably given our non-detections n sources with clear OH outflows. We note that any vagaries of gravitational lensing or differential magnification cannot explain the lack of highvelocity [CII] emission: each source shows high-velocity OH absorption, which must necessarily be down-the-barreand share essentially the same magnification as the dust continuunive find best estimates forthe molecularoutflow masses for Even if the [CII] traces a more extended odiffuse outflow component, the portion along our line of sight would still have been detectable just as the OH was. We also note that the highparagraph is solely forthe atomic phase this would require velocity [CII] found by Ginolfi et al. (2020) in stacked images is compact and centered on the galaxies, while the core geometry. We consider a few other possible explanations for our lack of evidence for [QI] outflows.

First, none of the literature stacking resultstargeted nor necessarily includesDSFGs such as our objects; no clean comparison result for DSFGs is currently available. The stacking resultof Ginolfi et al. (2020) is the mostdifficult to rule out with our sample due to the intrinsically broader line profiles of our sourcesThe galaxies in that sample have both lower mass and lower SFR than our targets, and it seems unlikely that such objects would drive higher outflow rate or brighter outflows than our more extreme target leanwhile, the quasars of Bischetti et al. (2019) are probably fairly similar to our target galaxies in mass, but we have no evidence for AGN in any of our targets Perhaps the additional energy and momentum from an accreting black hole are required to boost the [CII] line wings to observable fluxes.

Second, most recent [IQ] outflow detections have relied on stacking low-S/N spectra of many objects which introduces additional complexity and uncertainty in the results. Given the lines toward 11 DSFGs selected from the SPT DSFG sample. faint line wings to be searched for and heterogeneity in the input objects, great care must be taken in the details of the stacking, including continuum subtraction, relative scaling, non-Gaussian line shapes in the input spectra, and the treatmentabsorption in all objects. The observations also spatially also explain the differences in the quasar sample stacking results in the literature even though these studies have many individual sources in common (Decarlet al. 2018; Bischetti et al. 2019; Stanley et al2019). It could also be that [QI] is rarely apparent in outflows, but when it is present it is unusually bright, such that the stacked signal seen in literature conclusions can be summarized as follows. studies is dominated by a few atypical objects.

Third, OH is in principle a far more sensitive tracer of weak outflows than [C II], mostly due to the fact that it is an absorption tracersensitive to column (rather than volume) density and the very high Einstein A coefficients of the doublet lines. While we consider it highly unlikely given the wealth of evidence for high line opacities at low redshift, if the OH absorption were optically thin, the OH data are sensitive to outflow masses as low as □~(2–6) □ \*M□ 1(Paper II). On the other hand, following the calculations of Hailey-Dunsheath et al. (2010), our [C II] data are sensitive to outflow masses

 $\sim$ (5–15) $\square \times \square' 1 M_{\odot}$ , or  $\square 5\%$  of the total molecular gas masses of these galaxies. These values are highly uncertain due to the unknown abundances of OH and C and the ionization fraction opacity, though still far lower than expected for OH; e.g., Gullberg et al. 2015).

Finally, [CII] is often stated to be a tracer of neutral atomic outflowing gas, and not necessarily of molecular material (although [QI] is known to be emitted in both these phases as well as ionized gas). Perhaps, then, the molecular gas dominates the mass budget of these outflows, with atomic gas a smaller contribution to the total outflow mass. In Paper II, these four sources  $\sim (40-80) \square \times \square M \Omega$ . If we assume that the sensitivity to outflow mass from [C II] in the previous molecular-to-atomic outflow mass ratios of ~5-10 to reconcile the [CII] and OH observations. While the distribution of mass systemic emission is more extended, as expected for a shell-likecross outflow phases is completely unknown for high-redshift DSFGs from observations, this range is not infeasible based on estimates from chemicahodeling in idealized hydrodynamic simulations (Richings & Faucher-Giguère 2018) or the few lower-redshift observational estimates (Feruglio et al. 2010; Rupke & Veilleux 2013; Herrera-Camus et al019).

> Regardless of the reason, our data make clear that [C II] should not be considered a reliable molecular outflow tracer. We find no evidence for excess [Cemission at the velocities where we see blueshifted OH absorption or excess emission at the level seen in literature stacking experimer frarther work is needed to determine exactly why [CII] does not always appear in outflows.

## 6. Conclusions

In this work we have presented the first statistical sample of molecular outflows observed in 4□<□z□<□5.5 DSFS@sg ALMA observations of the ground-state OH 119 µm doublet Our target galaxies, all of which are gravitationally lensed, are IR-luminous,  $\log(L_{\rm IR}/L_{\rm II}) > 12$ , but do not show obvious signs of AGN activity in rest-frame mid-IR data. We detect OH of differing line widths among input sources. These details may resolve the targets, and we create source reconstructions of the rest-frame 120 µm dustontinuum emission and the OH line absorption. These galaxies represent the largest sample at  $z\Box >\Box$ with constraints on the molecular outflow properties, as well as the largest (and so far only) sample to spatially resolve the structure of said outflows in the early universe. Our main

> 1. We find unambiguous evidence for molecular outflows in 8 of the 11 sample targets the remaining sources have broad CO or [0] line profiles that make interpretation of the OH absorption complicated. No source shows unambiguous evidence fomolecularinflows. The outflow detection rate, 73% □±□13%, is similar to that found from OH observations of nearby ULIRGs and QSOs and significantly higher than for lower-luminosity AGNdominated galaxiesat low redshift. Because outflows with OH are only detectable in absorption, this detection rate is a lower limit on the true occurrencerate of

must be ubiquitous and widespread in such objects (Figure 4 and Section 4.1).

- and possibly fasterThe distribution of outflow velocities in the z□>□4 sample is indistinguishable from thatredshift IR-luminous galaxies (Figure 5 and Section 4.2).
- 3. Using our lensing reconstructions of the sources, we measure the structure of the outflows on ~500 pc spatial scales. The covering fraction of the outflowing molecular 1607611. gas is correlated with both and outflow velocity, such that more luminous sources and those with the fastest fractions (Figures 8 and 9).
- 4. The molecular outflows show significantly more clumpy structure than the (generally smooth) dust continuum emission on scales of ~500 powhich we quantify with metrics borrowed from the literature on high-redshift star formation (Figure 10 and Section 4.4). While the clumps are not directly resolved from optical depth arguments we expect that higher-resolution observations of the outflows would revealsubstantially more clumpy structure on 50-200 pc spatial scales (Figure 11 and Section 5.1).
- 5. We find no evidence of high-velocity wings in the [C] line profiles of the four sources with high-quality [QI] spectra and obvious OH outflows; [CII] is at best an unreliable indicator of molecular outflowsWe strongly rule out [C II] line wings at the level reported in several literature stacking results (though none explicitly targeted (Hunter 2007). high-redshift DSFGs similar to our sample). This may be due to lingering systematics in the stacking results or genuine differences between the [Coutflow properties of DSFGs like our sample and the variety of objects for which [CII] outflows have been claimed (Figure 12 and Section 5.2).

This work has largely focused on the structural properties of the OH outflows we have detected. In the second paper in this described in Section 3.3the lensing potentialn each source series we explore the physical roperties of these outflows in much greaterdetail, including outflow rates and masses and implications for the outflow driving mechanisms. Moreover, the outflow occurrence rate, velocity distributions, and detailed parameters). structural properties we find place novel observational constraints on simulations of galactic feedback and winds in the early universeWhile clearly a larger high-redshift sample fully understand galactic winds in the distant universe, this sample represents a firstep toward understanding outflow properties among the generaligh-redshiftgalaxy population and the utility of OH absorption for characterizing these properties in statistical samples.

that improved the quality of this paper. J.S.S. thanks the McDonald Observatory athe University of Texas at Austin for support through a Harlan J. Smith Fellowship and the Texas Advanced Computing Center(TACC) for providing

molecular outflows in z > 4 DSFGs; molecular outflowshigh-performance computing resources. S.is supported by NASA Hubble Fellowship grant #HF2-51446 awarded by the Space Telescope Science Institute hich is operated by the 2. The outflows reach maximum velocities of 430–1200 km Association of Universities for Research in Astronomylnc., for NASA, under contract NAS5-26555K.C.L., S.J., D.P.M., K.P., and J.D.V. acknowledge support from the US NSF under grants AST-1715213 and AST-1716127. This work was performed in partat the Aspen Centerfor Physics, which is supported by National Science Foundation grant PHY-

This paper makes use of the following ALMA data: ADS/JAO. ALMA#2015.1.00942.S, ADS/JAO.ALMA#2016.1.00089.S, outflows also host the outflows with the highest covering ADS/JAO.ALMA#2016.1.01499.S,ADS/JAO.ALMA#2018. 1.00191.S, and ADS/JAO.ALMA#2019.1.00253.S. ALMA is a partnership of ESO (representing its member states), NSF (USA) and NINS (Japan),togetherwith NRC (Canada),MOST and ASIAA (Taiwan), and KASIRepublic of Korea), in cooperation with the Republic of Chile. The Joint ALMA Observatory is operated by ESOAUI/NRAO, and NAOJ. The National Radio Astronomy Observatory is facility of the National Science Foundation operated under cooperative agreement by Associated Universities, Inc.

> This research has made use of NASA's Astrophysics Data System.

Facility: ALMA.

Software: CASA (McMullin et al. 2007), visilens (Spilker et al. 2016b), ripples (Hezaveh et al. 2016), astropy (Astropy Collaboration et al. 2018), matplotlib

# Appendix Supplementary Lens Model Results

This appendix provides additional results and diagnostic plots from the lens modeling procedure.

Table A1 lists the best-fit lens model parameters.As is parameterized as one or more SIE mass profiles with optional external tidal shear and low-order angular multipoles (see Hezaveh etal. 2016 for a more thorough description of these

Figure A1 shows the data, model, and residuals from the lens modeling for the 119 µm continuum.

Figure A2 shows the effective FWHM resolution of the that spans a wider range in galaxy properties will be required tensing reconstructions as a function of position in the source plane. These maps were made from reconstructions of mock data analyzed in the same way as the real data; see Section 3.3.1. These images show the resolution for the 119 µm continuum reconstructions. A similar exercise with the noise properties of the frequency ranges of the OH absorption components in each source gives nearly identical results. These We thank the referee for a thorough and constructive report maps make intuitive sense in that regions near the caustics with high magnification correspond to bettesource-plane resolution. We find good agreement with the usual rule of thumb that source-plane resolution is approximately the data resolution divided by the square root of the local magnifition.

Table A1
Best-fit Lens Model Parameters

Source	Δx	Δy	$log(M ( < 10 \text{ kpg})/M_{\square})$	e <sub>x</sub>	e <sub>y</sub>	Source	Υx	Yy	A <sub>3</sub>
SPT0202-61	+0.016□±□0.004	+0.070□±□0.002	11.221□±□0.010	+0.22□±□0.07	-0.53□±□0.13	SPT0202-61	+0.281□±□0.007	+0.074□±□0.004	0.087□±□0.005 0.
SPT0418-47	+0.097□±□0.004	-0.019□±□0.004	11.537□±□0.005	+0.09□±□0.02	-0.23□±□0.10	SPT0418-47	0.000□±□0.005	-0.011□±□0.005	L
SPT0441-46	+0.079□±□0.010	+0.338□±□0.007	11.385□±□0.013	+0.03□±□0.04	-0.19□±□0.06	SPT0441-46	-0.074□±□0.019	-0.019□±□0.025	-0.086□±□0.013 0.
SPT0459-58	-0.068□±□0.022	+0.045□±□0.018	10.994□±□0.025	+0.27□±□0.05	+0.01□±□0.05	SPT0459-58	L	L	L
	-0.378□±□0.023	+0.341□±□0.026	10.563□±□0.058	+0.53□±□0.07	-0.31□±□0.09				
SPT0459-59	-0.280□±□0.016	+0.699□±□0.016	11.246□±□0.034	+0.27□±□0.09	-0.12□±□0.07	SPT0459-59	-0.031□±□0.022	-0.032□±□0.043	L
SPT0544-40	-0.075□±□0.002	+0.056□±□0.003	11.055□±□0.010	+0.40□±□0.02	+0.26□±□0.02	SPT0544-40	-0.030□±□0.010	-0.085□±□0.012	L
SPT2048-55	-0.006□±□0.017	+0.007□±□0.016	11.020□±□0.007	+0.17□±□0.21	0.21□±□0.15	SPT2048-55	+0.067□±□0.119	+0.080□±□0.082	L
SPT2103-60	+0.851□±□0.005	-0.485□±□0.006	11.151□±□0.001	+0.42□±□0.02	-0.24□±□0.02	SPT2103-60	L	L	L
	+0.117□±□0.020	+1.113□±□0.021	11.161□±□0.002	+0.43□±□0.02	-0.45□±□0.02				
	-1.423□±□0.043	-1.839□±□0.149	11.022□±□0.003	+0.84□±□0.02	0.11□±□0.02				
SPT2132-58	-0.174□±□0.023	-0.031□±□0.014	10.874□±□0.003	-0.15□±□0.04	-0.74□±□0.05	SPT2132-58	+0.101□±□0.050	-0.035□±□0.036	L
SPT2311-54	-0.081□±□0.018	-0.345□±□0.026	10.657□±□0.003	+0.17□±□0.06	-0.45□±□0.08	SPT2311-54	L	L	L

Note. Parameter descriptions are as follows.  $\Delta x$ ,  $\Delta y$ : lens position in arcseconds relative to the ALMA phase  $\log(M_{\odot} < 10 \text{ kpg})/M_{\odot}$ : mass contained within 10 k components. y y: external tidal shear components, y y: m==3 multipole components. A m==4 multipole components. Entries with ellipses were fixed to 0 d (SPT0459-58 and SPT2103-60) list each lens; no shear or multipole parameters were used for these sources.

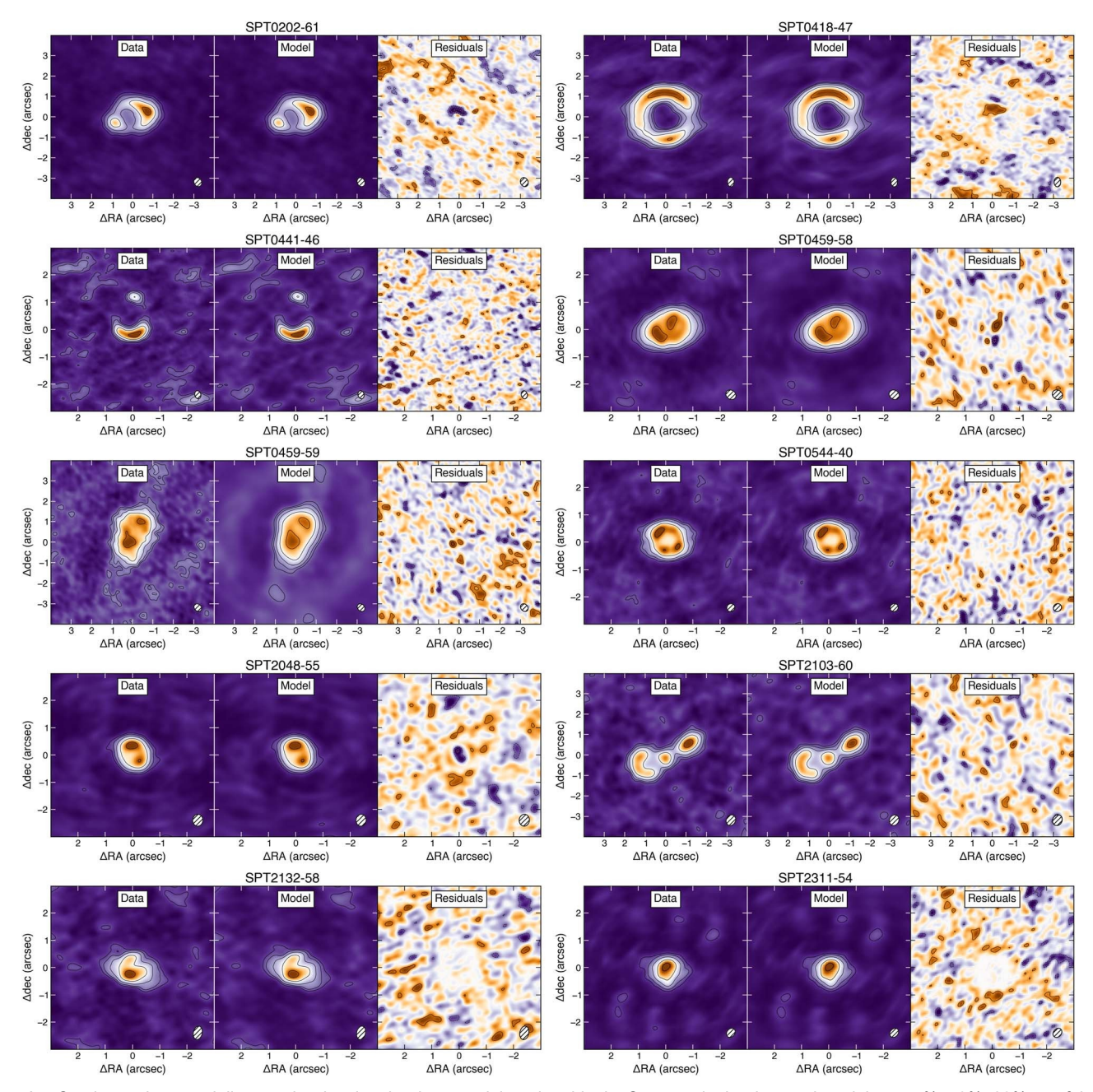


Figure A1. Continuum lens modeling results showing the data, model, and residuals. Contours in the data and models are 5%, 10%, 20%, ... of the peak, and cont in the residuals are in steps of ±2σ. Axes are relative to the ALMA phase center. Data and model images are dirty (not deconvolved) because the fitting is perform in the Fourier domain; the sidelobe structure resulting from the uv coverage of the observations in the data should be reproduced in the model. Emission from the lin SPT0202-61 and southwestern source in SPT0459-59 has been subtracted in the visibilities prior to the lens modeling (visible in Figure 2); it is clear from the residual maps that this subtraction is imperfect.

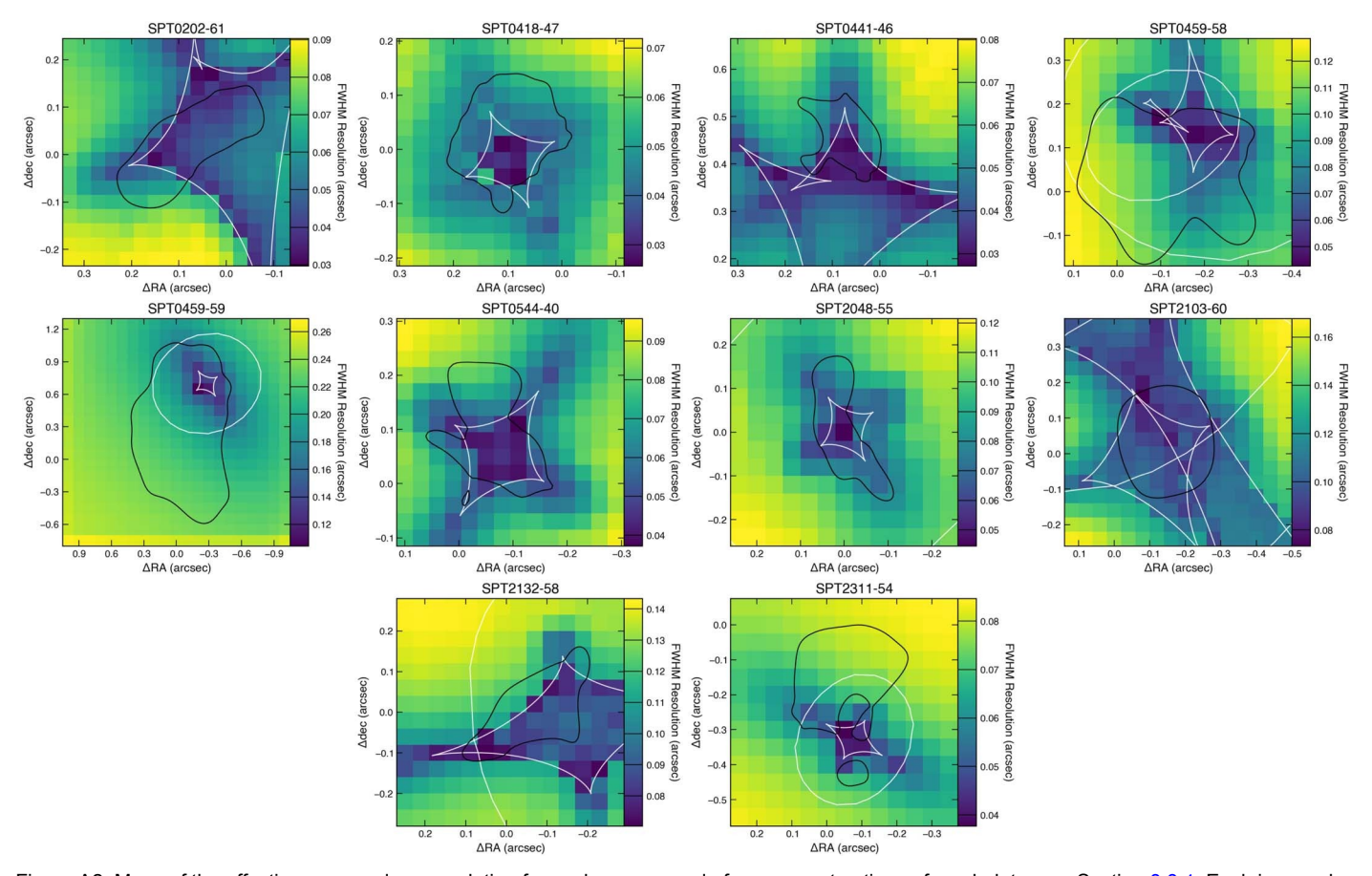


Figure A2. Maps of the effective source-plane resolution for each source made from reconstructions of mock data; see Section 3.3.1. Each image shows the FWHI a 2D Gaussian fit to the reconstruction of a pointlike artificial source at the center of each map pixel, "observed" and analyzed identically to the real data. Axes are relative to the ALMA phase centerThe black contour shows S/N□=□5 for the actual source as in FigWeite contours show the lensing caustics.

## ORCID iDs

Justin S.Spilker® https://orcid.org/0000-0003-3256-5615 Kedar A. Phadke® https://orcid.org/0000-0001-7946-557X Manuel Aravena® https://orcid.org/0000-0002-6290-3198 Matthieu Béthermin https://orcid.org/0000-0002-3915-2015 Chenxing Dong (董辰兴)https://orcid.org/0000-0002-5823-0349

Anthony H. Gonzale https://orcid.org/0000-0002-0933-8601 Christopher CHayward https://orcid.org/0000-0003-4073-3236

Yashar D.Hezaveh® https://orcid.org/0000-0002-8669-5733
Sreevani Jarugul® https://orcid.org/0000-0002-5386-7076
Katrina C. Litke ® https://orcid.org/0000-0002-4208-3532
Matthew A. Malkan® https://orcid.org/0000-0001-6919-1237
Daniel P. Marrone® https://orcid.org/0000-0002-2367-1080
Desika Narayana® https://orcid.org/0000-0002-7064-4309
Cassie Reute® https://orcid.org/0000-0001-7477-1586
Joaquin D.Vieira® https://orcid.org/0000-0001-7192-3871
Axel Weiss® https://orcid.org/0000-0003-4678-3939

### References

Abraham,R. G., van den Bergh,S., & Nair, P. 2003, ApJ, 588, 218
Alatalo, K., Blitz, L., Young, L. M., et al. 2011, ApJ, 735, 88
Aravena,M., Spilker,J. S., Béthermin,M., et al. 2016, MNRAS, 457, 4406
Astropy Collaboration

Banerji, M., Chapman S. C., Smail, I., et al. 2011, MNRAS, 418, 1071 Barcos-Muñoz L., Aalto, S., Thompson, T. A., et al. 2018, ApJL, 853, L28

Béthermin, M., De Breuck, C., Gullberg, B., et al. 2016, A&A, 586, L7 Béthermin, M., Fudamoto, Y., Ginolfi, M., et al. 2020, A&A, 643, A2 Bischetti, M., Maiolino, R., Carniani, S., et al. 2019, A&A, 630, A59 Boquien, M., Burgarella, D., Roehlly, Y., et al. 2019, A&A, 622, A103 Burgarella, D., Buat, V., & Iglesias-Páramo J. 2005, MNRAS, 360, 1413 Calderón, D., Bauer, F. E., Veilleux, S., et al. 2016, MNRAS, 460.3052 Capak, P. L., Carilli, C., Jones, G., et al. 2015, Natur, 522, 455 Carlstrom,J. E., Ade, P. A. R., Aird, K. A., et al. 2011, PA SP,123,568 Carnall, A. C., Walker, S., McLure, R. J., et al. 2020, MNRAS, 496, 695 Casey, C. M., Cooray, A., Killi, M., et al. 2017, ApJ, 840, 101 Chisholm, J., Tremonti, C. A., Leitherer, C., et al. 2015, ApJ, 811, 149 Cicone, C., Maiolino, R., Gallerani, S., et al. 2015, A&A, 574, A14 Decarli, R., Walter, F., Venemans B. P., et al. 2018, ApJ, 854, 97 Estrada-Carpenter, V., Papovich, C., Momcheva, I., et al. 2020, ApJ, 898, 171 Everett, W. B., Zhang, L., Crawford, T. M., et al. 2020, ApJ, 900, 55 Faisst, A. L., Schaerer D., Lemaux, B. C., et al. 2020, ApJS Falstad, N., Hallqvist, F., Aalto, S., et al. 2019, A&A, 623, A29 Fan, L., Knudsen, K. K., Fogasy, J., & Drouart, G. 2018, ApJL, 856, L5 Farrah, D., Lebouteiller, V., Spoon, H. W. W., et al. 2013, ApJ, 776, 38 Feruglio, C., Ferrara, A., Bischetti, M., et al. 2017, A&A, 608, A30 Feruglio, C., Maiolino, R., Piconcelli, E., et al. 2010, A&A, 518, L155 Fischer, J., Sturm, E., González-Alfonso E., et al. 2010, A&A, 518, L41 Forrest,B., Annunziatella,M., Wilson, G., et al. 2020, ApJL, 890, L1 Förster Schreiber, N. M., Shapley, A. E., Erb, D. K., et al. 2011, ApJ, 731, 65 Gallerani, S., Pallottini, A., Feruglio, C., et al. 2018, MNRAS, 473, 1909 García-Burillo, S., Combes, F., Ramos Almeida, C., et al. 2019, A&A, George, R. D., Ivison, R. J., Smail, I., et al. 2014, MNRAS, 442, 1877 Ginolfi, M., Jones, G. C., Béthermin, M., et al. 2020, A&A, 633, A90 Glazebrook, K., Schreiber, C., Labbé, I., et al. 2017, Natur, 544, 71 González-Alfonso, E., Fischer, J., Spoon, H. W. W., et al. 2017, ApJ, 836, 11 Guarnieri, P., Maraston, C., Thomas, D., et al. 2019, MNRAS, 483, 3060 Gullberg, B., De Breuck, C., Vieira, J. D., et al. 2015, MNRAS, 449, 2883 Guo, Y., Rafelski, M., Bell, E. F., et al. 2018, ApJ, 853, 108

Hailey-DunsheathS., Nikola, T., Stacey,G. J., et al. 2010, ApJL, 714, L162

```
Hayward, C. C., & Hopkins, P. F. 2017, MNRAS, 465, 1682
Heckman, T. M., Armus, L., & Miley, G. K. 1990, ApJS, 74, 833
Herrera-CamusR., Sturm, E., Graciá-CarpioJ., et al. 2020, A&A, 633, L4
Herrera-Camus, Tacconi, L., Genzel, R., et al. 2019, ApJ, 871, 37
Hezaveh,Y. D., Dalal, N., Marrone,D. P., et al. 2016, ApJ, 823, 37
Hezaveh, Y. D., Marrone, D. P., Fassnacht, C. D., et al. 2013, ApJ, 767, 132
Hodge, J. A., Smail, I., Walter, F., et al. 2019, ApJ, 876, 130
Hodge, J. A., Swinbank, A. M., Simpson, J. M., et al. 2016, ApJ, 833, 103
Hunter, J. D. 2007, CSE, 9, 90
Ivison, R. J., Richard, J., Biggs, A. D., et al. 2020, MNRAS, 495, L1
JanssenA. W., Christopher, N., Sturm, E., et al. 2016, ApJ, 822, 43
Jones, G. C., Maiolino, R., Caselli, P., & Carniani, S. 2019, A&A, 632, L7
Klein, R. I., McKee, C. F., & Colella, P. 1994, ApJ, 420, 213
Kormann, R., Schneider P., & Bartelmann, M. 1994, A&A, 284, 285
Krieger, N., Bolatto, A. D., Walter, F., et al. 2019, ApJ, 881, 43
Langer, W. D., Velusamy, T., Pineda, J. L., Willacy, K., & Goldsmith, P. F.
  2014, A&A, 561, A122
Law, D. R., Steidel, C. C., Erb, D. K., et al. 2007, ApJ, 656, 1
Le Fèvre, O., Béthermin, M., Faisst, A., et al. 2020, A&A, 643, A1
Leroy, A. K., Walter, F., Martini, P., et al. 2015, ApJ, 814, 83
Litke, K. C., Marrone, D. P., Spilker, J. S., et al. 2019, ApJ, 870, 80
Lotz, J. M., Primack, J., & Madau, P. 2004, AJ, 128, 163
Lutz, D., Sturm, E., Janssen A., et al. 2020, A&A, 633, A134
Maiolino, R., Gallerani, S., Neri, R., et al. 2012, MNRAS, 425, L66
Marrone, D. P., Spilker, J. S., Hayward, C. C., et al. 2018, Natur, 553, 51
McCourt, M., Oh, S. P., O'Leary, R., & Madigan, A.-M. 2018, MNRAS,
McMullin, J. P., Waters, B., Schiebel, D., Young, W., & Golap, K. 2007, in
   ASP Conf. Ser. 376, Astronomical Data Analysis Software and Systems
   XVI, ed. R. A. Shaw, F. Hill, & D. J. Bell (San Francisco, CA: ASP), 127
Meléndez, M., Veilleux, S., Martin, C., et al. 2015, ApJ, 804, 46
Mocanu, L. M., Crawford, T. M., Vieira, J. D., et al. 2013, ApJ, 779, 61
NarayananD., Turk, M., Feldmann, R., et al. 2015, Natur, 525, 496
Nelson, E. J., van Dokkum, P. G., Förster Schreiben, M., et al. 2016, ApJ,
   828, 27
Planck Collaboration, Ade, P. A. R., Aghanim, N., et al. 2016, A&A, 594, A13
Popping, G., Decarli, R., Man, A. W. S., et al. 2017, A&A, 602, A11
Reuter, C., Vieira, J. D., Spilker, J. S., et al. 2020, ApJ, 902, 78
Richings, A. J., & Faucher-Giguère C.-A. 2018, MNRAS, 474, 3673
Rujopakarn,W., Daddi, E., Rieke, G. H., et al. 2019, ApJ, 882, 107
Runco, J. N., Malkan, M. A., Fernández-Ontiverosl, A., Spinoglio, L., &
   Pereira-Santaellal. 2020, arXiv:2009.07293
Rupke, D. S., Veilleux, S., & Sanders, D. B. 2005, ApJ, 632, 751
Rupke, D. S. N., & Veilleux, S. 2013, ApJL, 775, L15
Scannapieco E. 2013, ApJL, 763, L31
```

```
Schechter A. L., & Casey, C. 2018, RNAAS, 2, 228
Schneider E. E., & Robertson, B. E. 2017, ApJ, 834, 144
Schneider E., Robertson B. E., & Thompson, T. A. 2018, ApJ, 862, 56
Shao, Y., Wang, R., Jones, G. C., et al. 2017, ApJ, 845, 138
Snyder,G. F., Hayward,C. C., Sajina,A., et al. 2013, ApJ, 768, 168
Spiegelhalter D. J., Best, N. G., Carlin, B. P., & Van Der Linde, A. 2002,
   Journal of the Royal Statistical Society Series 64, 583
Spilker, J. S., Aravena, M., Béthermin, M., et al. 2018, Sci, 361, 1016
Spilker, J. S., Aravena, M., Marrone, D. P., et al. 2015, ApJ, 811, 124
Spilker, J. S., Aravena, M., Phadke, K. A., et al. 2020, ApJ, 905, 86
Spilker, J. S., Bezanson R., Marrone, D. P., et al. 2016a, ApJ, 832, 19
Spilker, J. S., Bezanson, R., Weiner, B. J., Whitaker, K. E., & Williams, C. C.
  2019, ApJ, 883, 81
Spilker, J. S., Marrone, D. P., Aguirre, J. E., et al. 2014, ApJ, 785, 149
Spilker, J. S., Marrone, D. P., Aravena, M., et al. 2016b, ApJ, 826, 112
Spinoglio, L., Malkan, M. A., Smith, H. A., González-Alfonso, E., &
  Fischer, J. 2005, ApJ, 623, 123
Spoon, H. W. W., Farrah, D., Lebouteiller, V., et al. 2013, ApJ, 775, 127
Stanley, F., Jolly, J. B., König, S., & Knudsen, K. K. 2019, A&A, 631, A78
Stone, M., Veilleux, S., Meléndez, M., et al. 2016, ApJ, 826, 111
StraatmanC. M. S., Labbé, I., Spitler, L. R., et al. 2014, ApJL, 783, L14
Strandet, M. L., Weiss, A., Vieira, J. D., et al. 2016, ApJ, 822, 80
Sturm, E., González-Alfonso E., Veilleux, S., et al. 2011, ApJL, 733, L16
Suyu, S. H., Marshall, P. J., Hobson, M. P., & Blandford, R. D. 2006,
          S. 371, 983
Tacchella, S., Carollo, C. M., Förster Schreiber, N. M., et al. 2018, ApJ,
Tacchella, S., Carollo, C. M., Renzini, A., et al. 2015, Sci, 348, 314
Tadaki, K.-i., Genzel, R., Kodama, T., et al. 2017, ApJ, 834, 135
Talia, M., Pozzi, F., Vallini, L., et al. 2018, MNRAS, 476, 3956
Thompson, T. A., & Krumholz, M. R. 2016, MNRAS, 455, 334
Valentino, F., Tanaka, M., Davidzon, I., et al. 2020, ApJ, 889, 93
Veilleux, S., Maiolino, R., Bolatto, A. D., & Aalto, S. 2020, A&ARv, 28, 2
Veilleux, S., Meléndez, M., Sturm, E., et al. 2013, ApJ, 776, 27
Vieira, J. D., Crawford, T. M., Switzer, E. R., et al. 2010, ApJ, 719, 763
Vieira, J. D., Marrone, D. P., Chapman, S. C., et al. 2013, Natur, 495, 344
Walter, F., Bolatto, A. D., Leroy, A. K., et al. 2017, ApJ, 835, 265
Walter, F., Weiss, A., & Scoville, N. 2002, ApJL, 580, L21
Warren, S. J., & Dye, S. 2003, ApJ, 590, 673
Weiner, B. J., Coil, A. L., Prochaska J. X., et al. 2009, ApJ, 692, 187
Weiß, A., De Breuck, C., Marrone, D. P., et al. 2013, ApJ, 767, 88
Weiß, A., Walter, F., Downes, D., et al. 2012, ApJ, 753, 102
Wuyts, S., Förster Schreiber, M., Genzel, R., et al. 2012, ApJ, 753, 114
Zhang, Z.-Y., Ivison, R. J., George, R. D., et al. 2018, MNRAS, 481, 59
Zubovas,K., & King, A. R. 2014, MNRAS, 439, 400
```